Space Sci Rev (2020) 216:16
https://doi.org/10.1007/s11214-020-0641-7

Quiet, Discrete Auroral Arcs—Observations

T. Karlsson[1] · L. Andersson[2] · D.M. Gillies[3] · K. Lynch[4] · O. Marghitu[5] · N. Partamies[6,7] · N. Sivadas[8] · J. Wu[3]

Received: 13 June 2019 / Accepted: 28 January 2020 / Published online: 5 February 2020

Abstract Quiet, discrete auroral arcs are an important and fundamental consequence of solar wind-magnetosphere interaction. We summarize the current standing of observations of such auroral arcs. We review the basic characteristics of the arcs, including occurrence in time and space, lifetimes, width and length, as well as brightness, and the energy of the magnetospheric electrons responsible for the optical emission. We briefly discuss the connection between single and multiple discrete arcs. The acceleration of the magnetospheric electrons by high-altitude electric potential structure is reviewed, together with our current knowledge of these structures. Observations relating to the potential drop, altitude distribution and lifetimes are reviewed, as well as direct evidence for the parallel electric fields of the acceleration structures. The current closure in the ionosphere of the currents carried by the auroral electrons is discussed together with its impact on the ionosphere and thermosphere. The connection of auroral arcs to the magnetosphere and generator regions is briefly touched upon. Finally we discuss how to progress from the current observational status to further our understanding of auroral arcs.

Keywords Discrete auroral arcs · Auroral acceleration region · Ionospheric currents

Auroral Physics
Edited by David Knudsen, Joe Borovsky, Tomas Karlsson, Ryuho Kataoka and Noora Partmies

✉ T. Karlsson
tomas.karlsson@ee.kth.se

1 Space and Plasma Physics, KTH Royal Institute of Technology, 10405 Stockholm, Sweden

2 Laboratory for Atmospheric and Space Physics, University of Colorado Boulder, Boulder, CO, USA

3 Department of Physics and Astronomy, University of Calgary, Calgary, Alberta, Canada

4 Department of Physics and Astronomy, Dartmouth College, Hanover, NH, USA

5 Institute for Space Sciences, Bucharest, Romania

6 Department of Arctic Geophysics, The University Centre in Svalbard, Longyearbyen, Norway

7 Birkeland Centre for Space Science, Bergen, Norway

8 Boston University, Boston, MA, United States

1 Introduction

The bright, visible aurora (often >1 kR) is most frequently aligned with the local magnetic field, with sharp emission boundaries resulting in the notion of 'discrete' aurora (Davis 1978). This emission can be stable for tens of minutes or dance around the sky at high speed with different colors associated with it (Akasofu 1965; Hanna and Anger 1971). The more dynamic 'discrete' aurora is most of the time related to Alfvénic acceleration (Colpitts et al. 2013) while the more stable (minutes to hours) emissions are caused by electrons accelerated by a quasi-static electric potential structure. This stable emission is often also called the 'inverted-V' type of aurora due to the signature in the early satellite electron spectrograms. The focus of this paper is the latest findings on the discrete, inverted-V, stable auroral arcs.

Optically, the diffuse and discrete aurora can be difficult to separate, especially since both can have sharp emission gradients. Depending on viewing angles, optical resolution, temporal cadence and observational wavelength, the cause of the precipitating particles can be identified. However, by not having all these observations, available studies in the literature might not have been able to separate the two and the reader should therefore be cautious of limitations of statistical studies from ground (note that recent advances in multispectral imaging are helping to mitigate these limitations.) Using satellite data, the processes can be most of the time be well separated but the horizontal extent and the dynamics can be lost. When interpreting single-satellite observations without imagery observation context, it is often assumed that the auroral arcs are in the east-west direction, while in reality the satellite might have crossed an auroral fold, spiral or other deviation from that simplified geometry. For this review we have decided to define a quiet discrete arc as an auroral phenomenon, which is associated with a upward field aligned current (FAC), emissions caused by accelerated precipitating particles (being more energetic than the thermal energy of the particles on the associated magnetic field line), and is temporarily stable (longer than the bounce time of an Alfvén wave on that magnetic field line, which is of the order of minutes, Vogt 2002).

The last decade has seen significant improvements in auroral imager performance and the number of all-sky stations. Using these improved observations, the knowledge of the characteristics of the quiet discrete arc has improved and is presented in Sect. 2. We now have access to high-resolution and often multiple satellite observations of the precipitation particles. This has led to improved understanding of the two dimensional aspects of the stable arc and its temporal evolution, which is presented in Sect. 3. With multiple point observation and using different instrumentation the latest understanding of the horizontal dynamics is presented in Sect. 4. Stable arcs can filament and evolve into multiple arcs. Recently significant progress has been made within this topic, which is discussed in Sect. 5. The aurora is not only a beautiful manifestation of the dynamics in the magnetosphere, but it also modifies the ionosphere. This effect is discussed in Sect. 6, while the driving magnetospheric sources are discussed in Sect. 7.

As demonstrated by this review, auroral physics is still a highly active research field and new types of satellite missions are needed, especially to increase our understanding of temporal and spatial variations. Only then can we fully understand the interaction between the ionosphere and magnetosphere. Section 8 highlights some of the measurements and questions that need to be addressed in the near future.

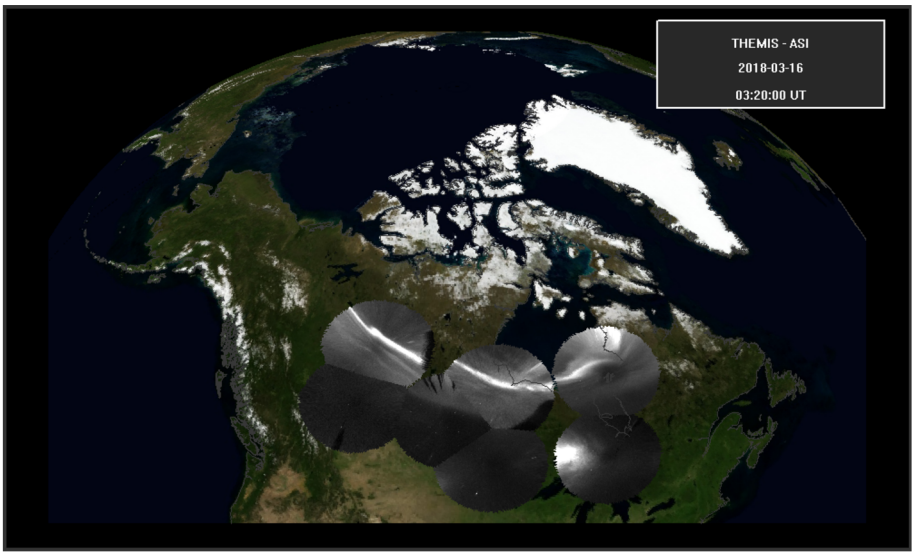

Fig. 1 An all-sky image mosaic of an example of typical quasi-stable arc captured by the panchromatic THEMIS cameras (Donovan et al. 2008) on 16 March, 2018, at 03:20 UT

2 Basic Characteristics

This section gives a comprehensive overview on recent findings framing the basic characteristics and appearance of quiet quasi-stable auroral arcs, such as where and when quiet arcs are likely to be found, their physical parameters (size, duration, brightness), and associated electron precipitation energies. Detailed understanding of these basic parameters is important as the knowledge of arc morphology places strong constraints on arc generation theories. Quiet arcs, as defined by Davis (1978), are highly magnetic east-west elongated discrete auroral forms with lengths of 100–1000 km. The arc luminosity experiences a sharp lower altitude boundary. In general, the emission within the arcs is limited to altitudes between 80 and 400 km, with a peak around 110 km (Davis 1978). Here we consider "quiet" to refer to arcs occurring under low, typically less than $Kp = 4$, geomagnetic conditions. These can be growth phase arcs prior to the substorm onset (see Fig. 1) or high-latitude arcs, which map to the plasma sheet boundary layer.

2.1 Arc Occurrence

In order to accurately describe quiet auroral arcs it is helpful to first identify the large scale parameters such as when and where this type of aurora occurs.

Latitudinal Variation For the purposes of this review, the nightside auroral oval is defined as the region of closed geomagnetic field lines located equatorward of the "red-line shelf" and poleward of the optical "b2i" boundary. The "redline shelf" is used to identify the poleward boundary of soft-electron precipitation which generally marks the boundary of the polar cap (a region of open geomagnetic field lines, Blanchard et al. 1995, 1997; Wanliss et al. 2000; Johnsen and Lorentzen 2012). Alternately the optical "b2i" boundary is a visual manifestation of the equatorward boundary of the proton aurora corresponding

to a transition from strong pitch angle scattering to bounce trapped particles (Jayachandran et al. 2002; Donovan et al. 2003). This is a reasonable definition in the context of this paper, since discrete auroral arcs are believed to be found exclusively poleward of the b2i boundary (Lyons et al. 1988; Newell et al. 1996). At present time, there is a lack of studies applying this definition to the dayside auroral oval. Thus, for the purpose of this review we refer to the nightside here. With these definitions in mind, quiet discrete arcs are generally found within the oval, between about 60–80 degrees geomagnetic latitude (MLat). Multiple studies have sought to capture the latitude range of quiet auroral arcs. Nevanlinna and Pulkkinen (2001) used an all-sky imager (ASI) network located in Finland to perform a survey of over 100,000 hours of all-sky data. The study extended to all forms of aurora with quiet auroral arcs as a subset of their data. They specifically looked at the percentage of auroral occurrence (the chance of seeing a particular type of aurora) and concluded that the occurrence of quiet arcs peaked near 70° MLat. The high latitude positions of the cameras used in this study meant that it was difficult to firmly establish upper and lower boundaries which potentially confine stable arcs. Gillies et al. (2014) used the THEMIS ASI network to study over 7500 quiet auroral arcs. Using ASIs spanning the auroral oval, they surveyed the latitude extent of single and multiple arc systems. They found that the 2687 observed single arcs occurred under lower geomagnetic activity levels and were confined to a narrower latitude band (67–75° MLat) as compared to the multiple arcs. The approximately 5400 images containing multiple arcs expanded across a broader range of latitudes of 62–75° MLat.

Pre-existing growth phase arcs (a subset of quiet arcs) were studied by Jiang et al. (2012) by comparing FAST spacecraft and ground-based optical observations. They determined that these arcs were located at, or very near, the boundary between the Region 1 and Region 2 field-aligned currents. In two events, Nishimura et al. (2012) found the upward FAC of preonset arcs located within the downward R2 FAC near the midnight. Using measurements from AMPERE, Motoba et al. (2015) further established that these growth phase arcs were observed to appear about 4.3 degrees equatorward of the R1/R2 boundary. This separation was found to decrease to about 1 degree as substorm breakup approached.

Diurnal Variation While quiet and growth phase arcs are confined to a relatively narrow latitude band, they can be found at nearly all magnetic local times (MLT). Growth phase arcs tend to have a strong preference for the midnight sector. Considering that this particular type of arc is a pre-substorm growth phase feature, it is unsurprising that they have a strong disposition to occurring at 20–03 MLT (Kozlovsky et al. 2001; Jiang et al. 2015a). Quiet arcs occur across all MLTs. Green emission dominated arc-like aurora has been observed frequently in the pre- and post-noon sectors on the dayside (Hu et al. 2009), while the noon region has found to contain fewest arcs (Qiu et al. 2016). The statistical study by Gillies et al. (2014) separated quiet arcs into single and multiple arc systems. They found that single (multiple) quiet arcs were seen between 14 and 8 MLT with a peak occurrence near (23–24 MLT) 22–23 MLT. This is in agreement with a study by Syrjäsuo and Donovan (2004) which used machine learning to identify and catalogue auroral structures. They found that the prevalence of arcs (of which quiet arcs was a subset) peaked near 20–21 MLT. This is also seen in a study by Partamies et al. (2008) which found a statistical preference for the inverted-V structures seen by FAST, confirmed by ground-based optical signatures, to occur around 21–23 MLT.

Alignment One of the unique features of the quiet auroral arcs is their alignment along lines of constant geomagnetic latitude. While arcs have frequently been observed to exhibit this behavior few studies have sought to quantify and further explore this property. Gillies

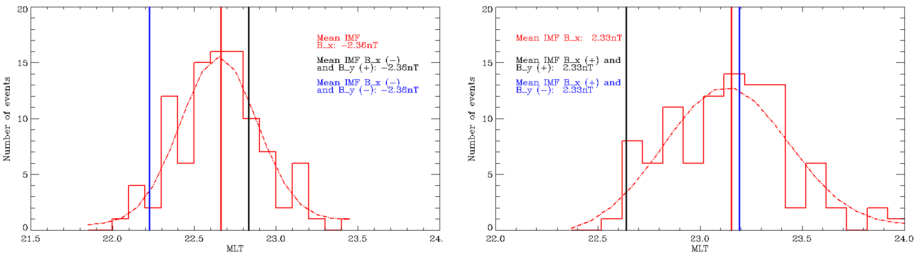

Fig. 2 Distributions of the single arc tilt reversal locations in MLT for subsets of about 100 events. IMF B_X negative (left) and positive (right) were investigated separately. The histograms give the observed reversal distribution to which the Gaussian (dashed red) was fitted to provide the MLT mean values of 22.6 and 23.1 (red vertical lines), respectively. Both datasets were further divided into cases of positive (black) and negative (blue) IMF B_Y. The same sign of B_X and B_Y moves the reversal duskward, while the opposite sign of B_X and B_Y twist the mean values dawnward. Figures from Gillies et al. (2014)

et al. (2014) performed one of the first large scale statistical studies quantifying the orientation of auroral arcs relative to the local magnetic east-west direction. Using five sites from the THEMIS ASI array, they identified over 7500 quiet arcs between the years 2007 and 2010 in images separated by at least 10 minutes. The sites chosen in this study provided a broad range of magnetic latitudes and longitudes designed to encompass a large portion of the auroral oval under different geomagnetic activity levels. One of the most notable results of this study was that stable auroral arcs are highly aligned with lines of constant geomagnetic latitude, indicating that their overall morphology is governed by the large-scale structure of the magnetosphere. In most cases the arcs were aligned (within $\pm 7.7°$) with lines of constant geomagnetic latitude. Interestingly, there was a clear relationship between the direction and magnitude of the arc tilt and MLT seen in three of the five stations presented. The tilt reversal is the point where arc alignment, as viewed along the structure from west to east, changes from equatorial to poleward tilt, on average. The reversal point for three stations occurred near the magnetic midnight, with the reversal point shifting toward the morning sector at higher latitudes. Tilt reversal behaviour resembles that of Harang discontinuity, but the relationship between these two phenomena needs further investigations. The reversal point had a strong MLT dependence on the interplanetary magnetic field (IMF) orientation. The orientation of the B_x and B_y components shifted the arc reversal by as much as half an hour in most cases. For example, if both B_x and B_y were positive (black on the right panel of Fig. 2) or both were negative (blue on the left panel of Fig. 2), the shift would be towards dusk. A combination of positive and negative orientations resulted in a slight shift dawnward. This tilt effect has also been observed on dayside. The combination of positive B_x and negative B_y shifted the tilt reversal towards midday, whereas negative B_x together with positive B_y moved the reversal point dawnward (Qiu et al. 2016).

Seasonal and Solar Cycle Variation A frequently asked question is how quiet arcs vary by the solar cycle and the Earth's seasons. However, few studies have properly addressed this. One of the earliest studies was performed by Nevanlinna and Pulkkinen (2001). Under the hypothesis of a good statistical correlation between auroral activity and solar cycle, they used all-sky camera images in northern Finland to categorize auroral arcs (among other auroral forms). While the overall total number of auroral observations was only weakly tied to the solar cycle they did find the number of quiet arcs anti-correlated with the sunspot number. This indicated that while active auroral forms were less frequent during solar minima,

quiet arcs were more common. Pulkkinen et al. (2011) recently furthered this idea by investigating the auroral electrojet evolution during the deep minimum at the end of the solar cycle 23 (2008–2009). One of the findings of this study was a confirmation of an increase in quiet arc occurrence during magnetically quiet periods. This is consistent with observations of downward accelerated electron beams (>5 mW/m^2), which occur twice as often during the solar minimum as compared to the solar maximum (Cattell et al. 2013). Partamies et al. (2014) used an automated auroral structure detection algorithm and performed a statistical study of the solar cycle dependence of arcs. Also in this study, quiet arcs were observed more frequently during the solar minimum years (specifically in 1996–1997 and in 2007).

From a ground-based perspective, seasonal studies are challenging as most auroral observations using ASIs require adequate dark conditions—a criterion fulfilled mostly in the winter season, particularly at high latitudes. The THEMIS array typically operates from late August to early April, similar to the high latitude stations of the Finnish all-sky imaging network. High-latitude stations, such as those on Svalbard, will observed the dark skies 24/7 from approximately November until February, but are still biased towards the winter season. Furthermore, dayside arc studies are very limited (Qiu et al. 2013; Hu et al. 2009). Thus, a vast majority of statistical studies are performed in the winter months, with September through March being preferred to avoid daylight complications. While not directly observing auroral arcs, there are a few studies of note which investigate the potential for auroral arc generation during winter and summer months. Newell et al. (1996a) used DMSP spacecraft to perform a survey of in-situ electron precipitation events and found that the occurrence rate of discrete aurora is lower during summer due to the increased probability of sunlit hours. Shortly after, Liou et al. (1997) analysed over 17,000 images acquired by the ultraviolet imager (UVI) on board the Polar satellite during the period of April–July 1996. Using these images, they calculated the N2 Lyman-Birge-Hopfield (LBH) auroral emission which can be used as a proxy for the total flux of precipitating electrons. Polar observations allowed monitoring of both hemispheres during the course of one orbit enabling the seasonal variation to be detected. This study concluded that discrete aurora was more common in the midnight sector in the dark hemisphere (winter) than in the sunlit hemisphere (summer). However, both of these studies included all discrete arcs, not just quiet arcs. One significant finding of this study was a link between seasons and geomagnetic activity levels. They attribute the gradual decrease in auroral emission on the nightside in the spring (April) to summer (July) months to this effect. While this study cannot distinguish between discreate and diffuse aurora, a later analysis of the same DMSP dataset (Newell et al. 2010) showed that the strongest monoenergetic precipitation comes to the pre-midnight sector, and that the winter time monoenergetic precipitation accounts for a higher energy flux compared to the summer scenario. More than the season, the precipitation energy flux was shown to be scaled by the solar wind. A further study of auroral electron precipitation was performed by Barth et al. (2004). They used the Student Nitric Oxide Explorer (SNOE) to determine the density of nitric oxide in the lower thermosphere—a marker of molecular nitrogen produced by auroral electron precipitation. An important result of their study was a clear seasonal dependence of precipitating auroral electron energy flux on the nightside at the energy of 4 keV marked by a minimum in electron flux (i.e. a reduction in NO production) as summer solstice was approached. They interpreted this to result from the high ionospheric conductivity which in the summer ionosphere suppresses the formation of auroral arcs. This seasonal dependence associated with auroral precipitation was investigated by Zheng et al. (2013) using a different approach: examining total hemispheric power (HP) calculated from satellite observations of the precipitating particle energy flux over the entire polar region. In this context, the precipitation related to quasi-static arcs is only part of the big picture. Nevertheless, they concluded

that the winter hemisphere receives more auroral power than the summer hemisphere during low geomagnetic activity levels. They also reported that the hemispheric asymmetry has a weak positive association with the solar cycle.

The above studies on seasonal variation in auroral arcs relied solely upon space-based observations of UVI aurora (for which there is limited resolution for resolving small scale quiet arcs) or focused on ionospheric electron precipitation patterns. When looking at the seasonal dependence from a ground-based perspective, one must also consider the effect of weather patterns which can impede statistical studies. In 2018, an as yet unpublished statistical survey of cloudiness was performed by D.M. Gillies and D. Chaddock at the University of Calgary. Using three key sites in the THEMIS ASI network (Fort Simpson, Fort Smith and Gillam) the effect of the local weather on the observing capabilities was determined. Gillies and Chaddock sampled images every 10 minutes during the time period of January–December 2014. Each viewing hour (the time for which the camera was on and operating) was divided into segments of 10 minutes and each 10 minute 'bin' was assigned one of the following designations: cloudy, clear, or unclassifiable data. The 'clear' designation included events for which there were clear skies present—independent of the presence of aurora or light pollution effects from objects such as the moon. The cloudy classification was used when approximately 20% or more of the field-of-view of the camera contained clouds. Unclassifiable data contained images for which there was significant light pollution from external sources or weather conditions such as snow on the dome or rain precluded classification. Each site was classified independently to avoid bias in the results. In total, over 50,000 images were analysed. The results showed that over central Canada, the best viewing months from a cloud perspective, are November through April (Fig. 3). Unsurprisingly the winter months (November–February) contained the most images for which adverse weather conditions (such as snow obscuring the dome) precluded observations.

2.2 Arc Dimensions

Width One well-studied arc parameter is the latitudinal width/thickness: a feature easily identified in single ASI images. Knudsen et al. (2001) studied all-sky images of over 3000 auroral arcs found within 5 degrees of magnetic zenith. Limiting the study to a narrow band near the zenith is a necessary criterion in order to avoid elongating the width due to the altitude extent of the emission curtain. They concluded that a typical green emission arc has a width of 18 ± 9 km. This finding was further supported by a study of six evening sector arcs which had a similar median thickness of 18 km (Aikio et al. 2002), and by a set of about 400 thin pre-onset arcs at the equatorward boundary of the auroral oval (Nishimura et al. 2011). In contrast, a study of over 180 pre-onset arcs showed somewhat larger scales with widths of 20–50 km (Jiang et al. 2015a). Interestingly, as described by Aikio et al. (2002), the region of enhanced northward electric field on the equatorward side of the arc spanned 1–4 times the width of the arc, while a more recent study of midnight sector arcs showed arc widths (about 1.5 degrees in latitude) comparable to the size of the region with a strong electric field (50–150 km) (Aikio et al. 2018).

In their study, Knudsen et al. (2001) raised a question on whether the 1 km scale sizes do not exist or whether they had just not been measured. The optical resolution of the equipment used in the previous arc width studies had a minimum resolution of around 1 km. As a response, a set of 500 thin arcs with widths of 0.5–1.5 km were reported by Partamies et al. (2010) from an imager with a narrower field-of-view and higher spatial resolution (Fig. 4). They thus concluded that the spectrum of auroral arc widths is continuous.

From an in-situ observational point of view, inverted-V acceleration widths have been observed to be wider (>1 degree) than the ionospheric arc widths (<1 degree, Yago et al.

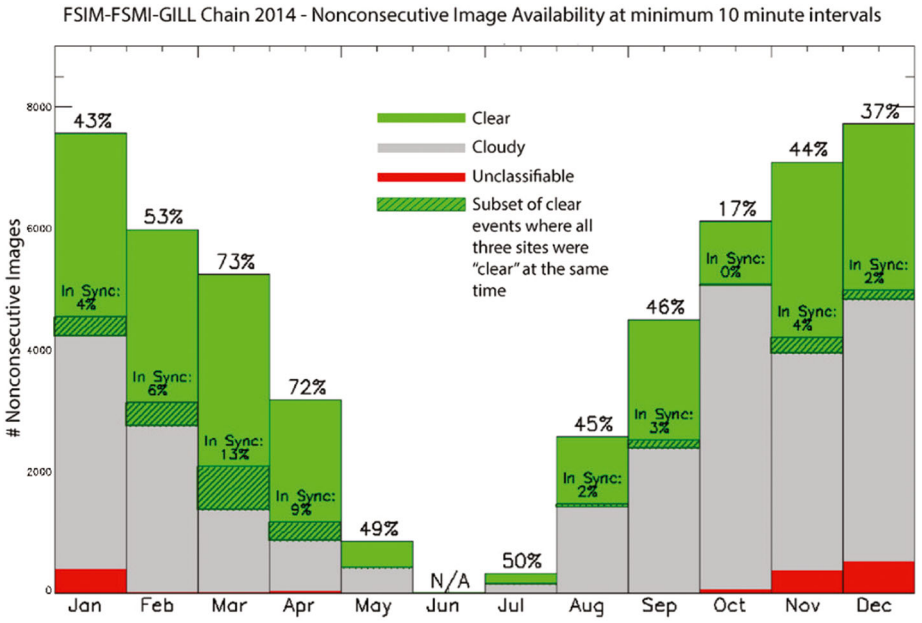

Fig. 3 Green indicates the time the camera was operating (as a percentage of the month), during which there were clear skies at an individual site to allow auroral observations. Grey represents cloudy conditions with zero chance of observing the aurora. The green hashed region demonstrates the percentage of time where the three adjacent sites (spanning approximately 3000 km) contain clear skies simultaneously, allowing large scale auroral observations

2005), suggesting that only higher energy electrons were able to produce observable emission. To further investigate this Partamies et al. (2008) conducted a statistical study of inverted-V structures as measured by the low-altitude orbiting FAST satellite. The typical acceleration potential was found 20–40 km wide, encompassing the ionospheric component of the arc. A more recent case study by Frey et al. (2010a) analysed an arc with an optical width of about 25 km and an inverted-V width of about 65 km. In agreement with the earlier results, they concluded that the optical emission with a limited width (25 km) was caused by the energy flux of the highest precipitation energies. The total energy flux input into the ionosphere, however, covered a larger region corresponding to the full width of the inverted-V precipitation.

Dayside arcs from the high-latitude Ny-Ålesund station were found to have comparable widths with the average of 18.5 km (Qiu et al. 2013), with the thinnest arcs closest to midday hours (at around 10 and 14 MLT). Post-midnight arcs, however, have been observed to have twice the scale (50–70 km) in association with low-energy precipitation of less than 200 eV (Aikio et al. 2004).

Length Less attention has been granted to the length of the auroral arcs, as that dimension is often limited by the camera field-of-view. The growth phase arcs have been concluded to extend over at least 0.75 hours in MLT (Lessard et al. 2007). Multiple studies have shown a soft upper limit of up to at least 2–5 hours in MLT (Donovan et al. 2008; Sergeev et al. 2012; Gillies et al. 2014; Nishimura et al. 2012).

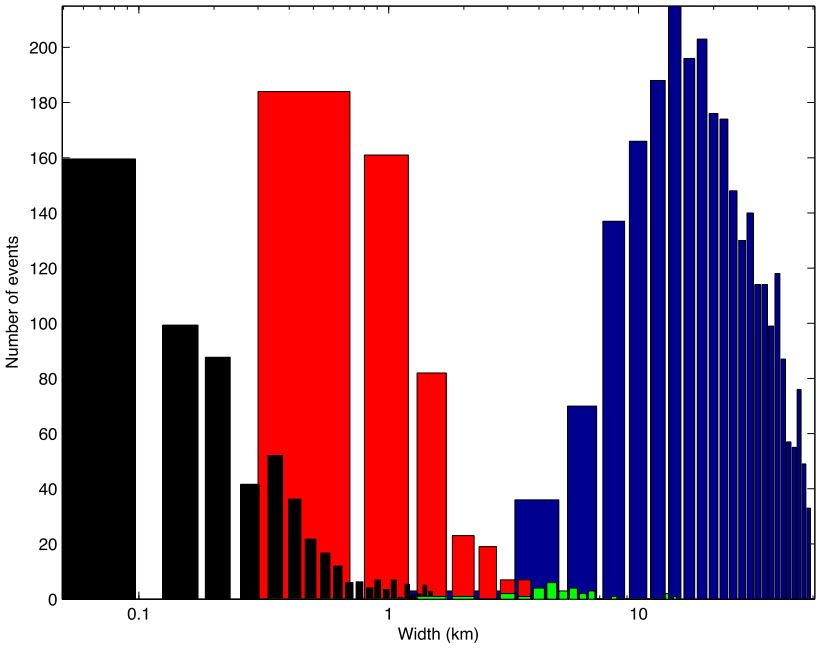

Fig. 4 A composite of observed arc widths based on ground-based studies. Auroral fine-scale observations by Maggs and Davis (1968) (black), meso-scale ASC observations by Knudsen et al. (2001) (blue) as well as widths captured by a 20-degree field-of-view by Partamies et al. (2010) (red). Some additional arc width observations are included from a short campaign through a 60-degree field-of-view (green). Figure from Partamies et al. (2010)

2.3 Brightness and Precipitation

The meso-scale (width of around 10–100 km, Partamies et al. 2010) arcs' peak intensities at the wavelength of 557.7 nm range from 0.2 to 200 kR with an average value of 15 kR (Knudsen et al. 2001). The peak brightness for an onset arc example by Frey et al. (2010a) at 427.8 nm was 3 kR. The brightness of the growth phase arcs has been observed to grow monotonically during the 4–5 minutes prior to the substorm onset (Lyons et al. 2002).

The precipitation energies of about 1 keV for high-latitude arcs (Safargaleev et al. 2003), 2–4 keV for inverted-V arcs (Partamies et al. 2008), 2.7 and 6 keV for quiet nightside arcs (Simon Wedlund et al. 2013), up to a few keV for pre-breakup arcs (Jiang et al. 2012) and several keV for pre-noon poleward moving arcs (Kozlovsky et al. 2003) have been reported. In the case of high-latitude arcs, the precipitation energy was seen to decrease with increasing distance to the auroral bulge (Safargaleev et al. 2003). These values are in a good agreement with the measured peak emission heights of 120–150 km (Sangalli et al. 2011; Qiu et al. 2013; Kozlovsky et al. 2003). The peak electron densities of evening sector arcs have been observed at the altitudes of 110–120 km, corresponding to a field aligned potential drop of about 1 kV (Aikio et al. 2002, 2018). In the events studied by Lessard et al. (2007), the inverted-V precipitation of the growth phase arc was gradually built up within the pre-existing diffuse precipitation (protons and electrons). In this case the peak energies stayed below 1 keV.

The typical electron energy fluxes of arcs were found to be 15–20 mW/m^2 (Partamies et al. 2004). Somewhat higher energies (12 keV) and energy fluxes (25 mW/m^2) were

observed for an onset arc by Frey et al. (2010a), while lower energy fluxes (less than 10 mW/m^2) were modelled from intensities measured by a camera on board the Reimei spacecraft (Whiter et al. 2012). In contrast, tall rayed arcs, which are accelerated by a combination of inverted-V's and Alfvén waves, were reported to have an order of magnitude lower peak energy flux of 1–3 mW/m^2 in correlation with the optical intensity (Hallinan et al. 2001). Correspondingly, the lower boundaries of the tall rays were found at higher altitudes (130–170 km) in agreement with precipitation energies of 100–800 eV. Similar heights of about 130 km were also observed for late morning (10 MLT) discrete arcs, corresponding to a Total Electron Content (TEC) variation of 10 TEC units and the line-of-sight electron density of 1.25×10^6 cm^{-3} (Kintner et al. 2002). It is also interesting that while these examples of soft precipitation spectra provide lower energy fluxes, there are also regions of Alfvénically accelerated aurora (such as poleward boundary regions) where the soft precipitation delivers very large energy fluxes, as discussed in Forsyth et al. (this issue).

Equatorward of and often overlapping with a growth phase arc, a band of high-energy precipitation with energies of 10–300 keV appears some minutes before the breakup (Deehr and Lummerzheim 2001; Shiokawa et al. 2005; Lessard et al. 2007; Sergeev et al. 2012). This high-energy band of diffuse emission is related to the D region electron density enhancement and thus, cosmic radio noise absorption (CNA) (Jussila et al. 2004; McKay et al. 2018), and was shown to consist of mainly protons (Lessard et al. 2007) with an emission intensity of 150–1000 R at 486.1 nm (Deehr and Lummerzheim 2001). The diffuse band was also observed to move equatorward with the thinner growth phase arc with a roughly constant separation of some tens of km (Deehr and Lummerzheim 2001; McKay et al. 2018).

Recent sounding rocket studies (Grubbs et al. 2018b,a; Clayton et al. 2019b) have made conjunction observations between filtered ground-based imagery at several wavelengths, and nightside auroral sounding rocket in situ observations of electron precipitation. These conjunctions help to test and improve inversion calculations of precipitation based on multispectral imagery observations. The rapidly increasing capabilities of cameras makes this a valuable and growing field of study, as these inversions can provide time-dependent two-dimensional maps of electron precipitation (both energy flux and characteristic energy).

2.4 Stability

Quiet growth phase arcs are often seen as quasi-stable structures with lifetimes up to several tens of minutes (e.g. Kozlovsky et al. 2001; Shiokawa et al. 2005; Lessard et al. 2007; Nishimura et al. 2011; Jiang et al. 2015a). As an example, a quiet evening sector arc was observed for 6 minutes for triangulation of the peak emission height by Sangalli et al. (2011). They found an average peak emission height for green emission at 120–140 km with a variation *along* the arc structure of about 40 km.

Comparing arc lifetimes across the substorm phases, Partamies et al. (2015) found, as expected, that the longest durations take place during the growth phases. The lifetimes in this study accounted for periods when the arcs were continuously detectable with a maximum gap of 40 seconds (1-image gap in a 20-second cadence). This criterion is sensitive to intensity variations, such as fading, and resulted in a typical lifetime of only 1–2 minutes for any single arc, and with 90% of the arc events lasting for less than 10 minutes.

Similarly, a large range of lifetimes have been reported for the high-altitude acceleration potential structures. These are discussed in Sect. 3.4.

2.5 Arc Drift and Plasma Flows

In Sect. 4 below we will consider the controlling factors for horizontal structuring of discrete arcs. Here we touch briefly on the signatures of their motion, and of the motion of plasma near them. The equatorward drift speeds of the growth phase arcs have been measured on the order of the ionospheric convection speed, 70–170 m/s (Deehr and Lummerzheim 2001; Aikio et al. 2002; Kozlovsky et al. 2001; Jussila et al. 2004; McKay et al. 2018), but sometimes also significantly faster, e.g. 250–650 m/s (Kozlovsky et al. 2003, 2006; Safargaleev et al. 2003). No clear distinction is found between the arcs drifting along or faster than the ionospheric convection flow. Very fast plasma flow channels have been identified in the low conductance regions next to the arc emission (and high conductance). For instance, Aikio et al. (2018) reported eastward plasma flow speeds of 3.3 km/s on the poleward side of a midnight sector arc, corresponding to southward electric field. Recent observations by the Swarm mission have solidified these observations of fast flows adjacent to discrete arcs. The strong prevalent flows reported by Archer et al. (2017) are referred to as Birkeland current boundary flows, as they are seen to be largest (exceeding 1 km/s) at the boundary between upward and downward field aligned currents. The extensive Swarm observations allow the distinction between these auroral boundary flows, and other ionospheric features such as subauroral ion drifts (SAID) (Archer and Knudsen 2018).

The shear flow direction in the morning sector is westward on the equatorward side and eastward on the poleward side of the arc (Jiang et al. 2015a). In addition, the arcs have been observed to expand azimuthally at approximately the shear flow speeds of about 1–5 km/s (Kozlovsky et al. 2003; Safargaleev et al. 2003; Shiokawa et al. 2005; Yago et al. 2005). The shear flow over arc precipitation allows smaller-scale vortical structures to grow within the arcs. This may drive magnetic reconnection in the auroral acceleration region above the arc (Chaston 2015) leading to a breakup of an unstable arc at the substorm onset.

3 High-Altitude Observations, Along and Perpendicular to B

There is considerable direct observational evidence that quiet, meso-scale arcs are associated with precipitating, accelerated electrons, e.g. early observations of emission line intensity ratios, indicating electron acceleration up to several keV (e.g Mende and Eather 1976; Christensen et al. 1987). As described above combined observations of optical arcs and accelerated electrons is further evidence (McIlwain 1960; Stenbaek-Nielsen et al. 1998; Kozlovsky et al. 2003; Frey et al. 2010a; Jiang et al. 2012; Simon Wedlund et al. 2013). The REIMEI spacecraft observations, including an onboard auroral imager and electron precipitation sensors, provided a detailed view of these relationships, as, for instance, in Motoba and Hirahara (2016). The extensive THEMIS GBO array (Mende 2008) provides an enormous data archive of imagery allowing conjunction studies with many spacecraft. One nice example is found in Archer et al. (2017). Others combine REIMEI and Themis-GBO (Frey et al. 2010b), FAST and Themis-GBO (Haerendel and Frey 2014; Haerendel et al. 2012), and Swarm and Themis-GBO (Liu et al. 2018b; Wu et al. 2017; Gillies et al. 2015). Sounding rocket studies (Grubbs et al. 2018b,a; Clayton et al. 2019b) with dedicated groundbased imagery provide additional conjunction studies.

Early on it was suggested that the precipitating electrons described in Sect. 2 were accelerated by electric fields above the aurora (e.g. McIlwain 1960; Evans 1968, 1974; Carlqvist and Boström 1970; Hallinan and Davis 1970). Observations of large electric fields perpendicular to the geomagnetic field above the aurora were taken as confirmation of this idea,

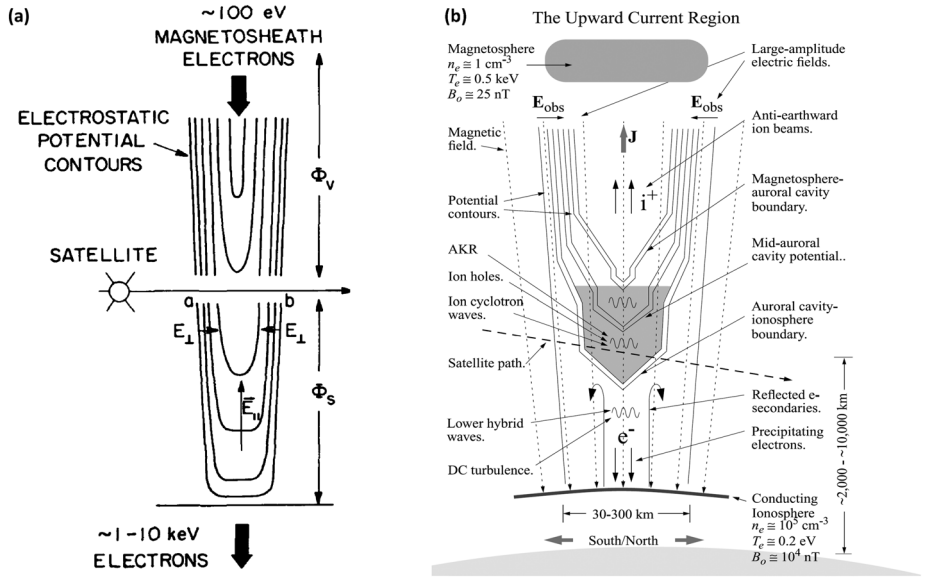

Fig. 5 Two interpretations of the U-shaped electric potentials above discrete auroral arcs. (**a**) Schematic adapted from Gurnett (1972) showing a potential structure with a relatively smoothly distributed $E_{\parallel}$. (**b**) Schematic from Ergun et al. (2004), where $E_{\parallel}$ to a large extent takes the form of localized double layers (see Sect. 3.4)

and were interpreted as a static, U-shaped electric potential structures, with an upward parallel electric field in the centre (Fig. 5a), based on measurements from the Injun-5 (Gurnett 1972) and S3-3 satellites (Mozer et al. 1977). These static electric potential structures are generally associated with the quiet arcs we discuss here (e.g. Marklund et al. 2011b; Li et al. 2013; Hull et al. 2016), and the central part with the upward-directed parallel electric field usually called the 'auroral acceleration region (AAR)'. More dynamic auroral forms can, on the other hand, be associated with time-varying electric fields associated with e.g. medium-frequency Alfvén waves. This type of acceleration is discussed in several companion papers in this issue. In this section we will discuss high-altitude observations associated with the static, U-shaped auroral acceleration potentials.

3.1 Overview

The basic configuration of the U-shaped electric potential structure, with converging perpendicular electric fields, has been confirmed by measurements from several satellites, such as DE-1 and 2 (Weimer et al. 1985), Viking (Block et al. 1987), FAST (McFadden et al. 1999), and Polar (Hull et al. 2003b). In particular the high-time resolution measurements from the FAST satellite have yielded detailed knowledge of the properties of the auroral acceleration region. An extensive review of results up until 2002 is given in the ISSI Auroral Plasma Physics book (Paschmann et al. 2003). We will mention some of them below, but will mostly focus on more recent results.

3.2 A Satellite Pass Above the Auroral Region

We will first briefly discuss a typical FAST pass above the auroral region, reproduced from Paschmann et al. (2003) and shown in Fig. 6. The current directions can be determined by

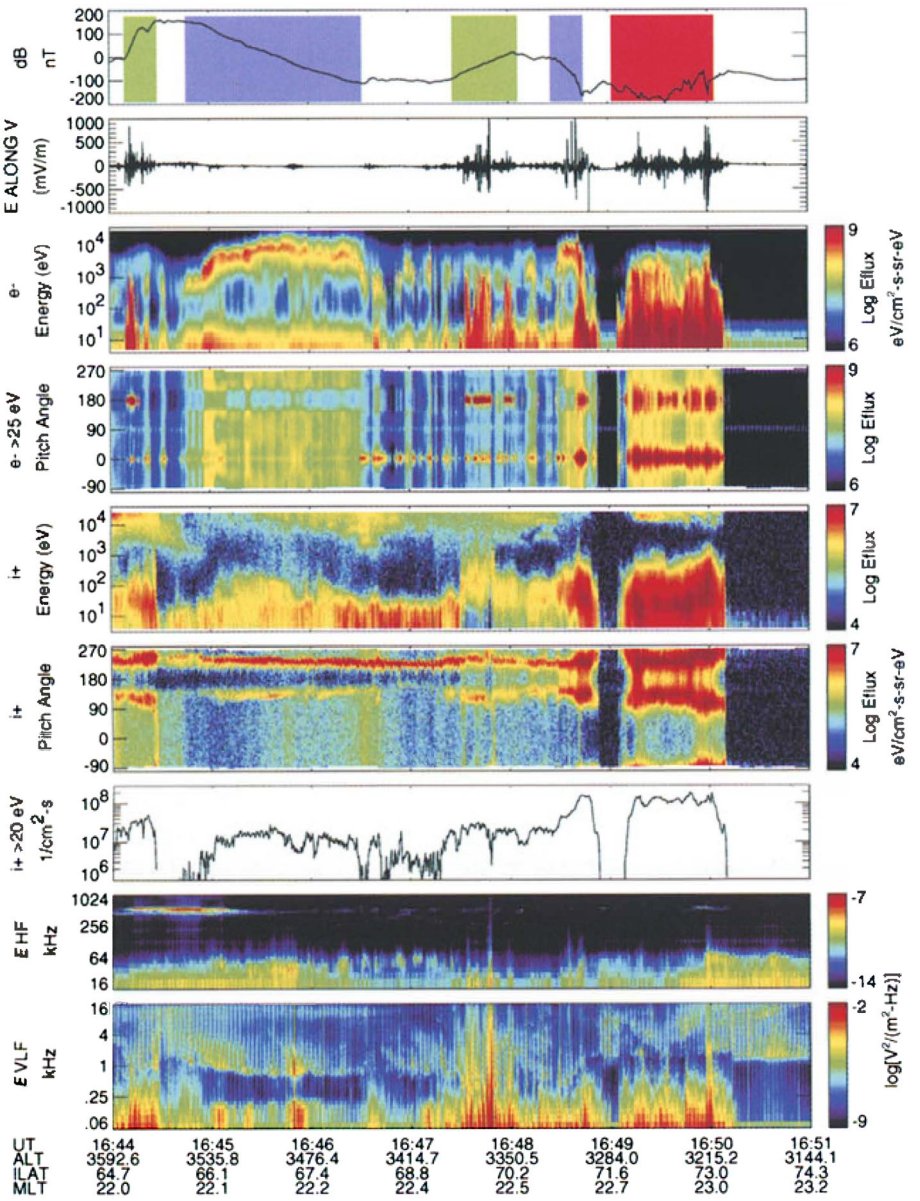

Fig. 6 A FAST satellite pass from the northern hemisphere auroral region. From top to bottom is shown east-west perturbation magnetic field *dB*, DC electric field, electron and ion spectrograms vs. energy and pitch angle, integrated upward ion flux, and electric field wave activity in two frequency intervals. Reproduced from Paschmann et al. (2003)

the gradient of *dB*, and are indicated in the figure: green for downward, purple for upward, and red for the changing current directions of the Alfvénic aurora, discussed by Forsyth et al. (this issue). The pass starts with a short traversal of a downward current region. Such regions will be discussed in Sect. 3.5. Between approximately 16:44:50 UT and 16:46:30

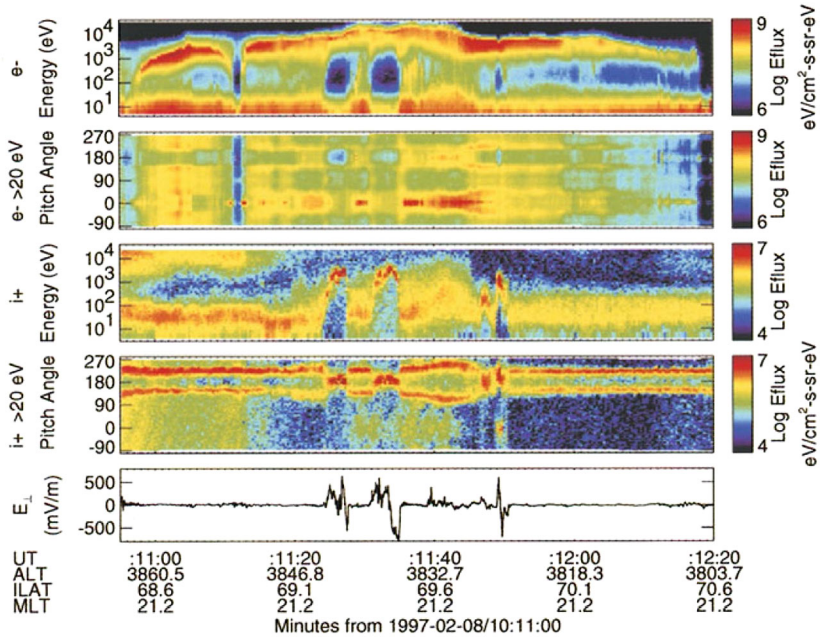

Fig. 7 A FAST pass across an upward current region. Adapted from (McFadden et al. 1999). From top to bottom is shown electron energy flux spectrograms versus energy and pitch angle, the same for ions, and the perpendicular (to the magnetic field) electric field

the spacecraft is inside a region of upward current. The electron measurements here show a typical signature of a large-scale inverted-V structure, being accelerated to maximum energies of close to 10 keV in the central current sheet. The lower energies of the electrons at the edges results in the typical inverted-V shape, and is consistent with electron acceleration by the U- (or 'V'-) shaped potentials shown in Fig. 5. This whole structure is also consistent with a large scale auroral arc, although the finer-scale structures in the electron inverted-V can correspond to individual smaller-scale arcs embedded inside the large arc (cf. Sect. 5). The high-energy electrons have a wide pitch-angle distribution, which reflects their plasma sheet origin. The low-energy population is a combination of ionospheric and atmospheric secondary electrons and photoelectrons emitted from the spacecraft. There is no sign of an upward accelerated ion beam in the upward current region, only ion conics created by transverse heating of ions and adiabatic transport along the field lines. This, together with the absence of large electric field signatures in association with the inverted-V boundaries, indicates that the spacecraft passes below the potential structure in this case. In contrast Fig. 7, from another FAST pass across an upward current region, shows clearly monoenergetically accelerated ion beams, also associated with very large electric fields. This is a consequence of the spacecraft being located above the lower border of the U-shaped potential structure for these times. Note that for these excursions into the auroral acceleration region, almost all of the low- and medium energy particles are absent. This is an example of the auroral density cavity, which will be discussed briefly below. These excursions into the AAR represent either small-scale spatial variations at its lower boundary ('auroral fingers', McFadden et al. 1999) or temporal variations of the position of the lower boundary.

3.3 Field-Aligned Current Sheets at High Altitude

There is long-standing proof that the auroral acceleration and precipitation takes place in regions of upward field-aligned current (Paschmann et al. 2003, and references therein). This is seen in terms of the large-scale Region-1 and -2 currents (Iijima and Potemra 1976), where the auroral oval emissions tend to take place in the Region-1 upward current in the premidnight region, and in the likewise upward-directed morningside Region-2 current (Paschmann et al. 2003). But above all, this is true on scales of individual auroral arcs and acceleration potential structures (where local small-scale upward currents can also be located within the general downward Region-1 and -2 current regions) (e.g. McFadden et al. 1999; Paschmann et al. 2003; Figueiredo et al. 2005). Johansson et al. (2007) studied the scales sizes of upward field-aligned currents and associated converging acceleration electric field structures, at an altitude of 4–7 R_E. They found scale sizes of 6.2 ± 2.6 km and 4.7 ± 0.45 km for the currents and electric fields, respectively, based on 85 Cluster observations of such structures.

The association between upward field-aligned current and upward-directed electric fields, accelerating electrons downward is consistent with the Knight relation (Knight 1973). This requires a parallel potential drop to allow the current carrying electrons overcome the mirror force and penetrate all the way to the ionosphere, where the currents can be closed by perpendicular ionospheric currents, maintaining current continuity. For a large range of field-aligned current densities this relation takes a linear form

$$j_{\parallel} = K U_{\parallel} \tag{1}$$

where $j_{\parallel}$ is the field-aligned current density, $U_{\parallel}$ is the total field-aligned potential drop, and K is the Knight or Lyons-Evans-Lundin constant (Knight 1973; Lundin and Sandahl 1978; Lyons et al. 1979). This is further discussed in the companion paper by Lysak et. al. (this issue).

The upward currents are often located close to and connecting to downward-directed field-aligned currents, constituting a balancing current, being connected via an ionospheric closure current, as described above (see also Sects. 4 and 3.5). Johansson et al. (2007) studied the scale sizes also of these currents at Cluster altitudes, and found similar mean and median scale sizes as for the upward currents. Notably this similarity of sizes is not seen in the lower ionosphere, where sounding rocket studies show downward current regions adjacent to arcs as being much narrower than their associated upward current neighbors (Lynch et al. 2015; Clayton et al. 2019b).

3.4 Structure of the Auroral Acceleration Potential

With single spacecraft measurements of the acceleration potential structures, it is difficult to disentangle temporal and spatial effects. With the Cluster spacecraft this is possible to some extent; a first example of this is the study by Marklund et al. (2011a), where the two-dimensional structure of the acceleration potential was revealed to consist of a two large U-potentials within a wider potential well, combined with an S-shaped potential (Fig. 8). One point made by the authors is that the scale sizes associated with the structure is very different when observed at different altitudes. Here we also introduce the S-shaped potential, which in contrast to the U-shaped one sustains a parallel electric field without uncoupling the perpendicular potential drop between the magnetosphere and the ionosphere (e.g. Mozer et al. 1980; Israelevich et al. 1988; Hwang et al. 2006b). The role of S-shaped potential structures in auroral acceleration is still unclear as their relative occurrence compared to U-shaped structures has not been established.

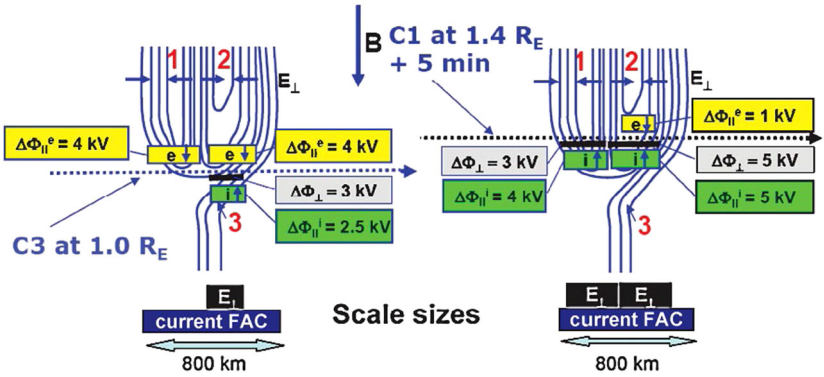

Fig. 8 Two-dimensional structure of the acceleration potential, based on measurements from Cluster 1 and 3 which passed through the potential structure with a time separation of five minutes, and a altitude separatin of 0.4 R_E. (Marklund et al. 2011a). Shown are equipotential structures (separation 1 kV), the widths of the down-going electron and up-going ion distributions (small yellow and green boxes), and estimates acceleration potentials (larger boxes). The potential estimates are based on upgoing ion energies (green), integrated perpendicular electric field (grey), and downgoing electrons (yellow). The width of the upward current region is indicated by the blue boxes, and the black lines and boxes indicate where the measured electric potential deviated appreciably from the ambient level

Many observations indicate that the potentials show considerable internal structure (e.g. Mozer and Kletzing 1998; McFadden et al. 1999; Hull et al. 2003b; Marklund et al. 2011a; Alm et al. 2015). Such internal structure may be due to spatial variations in the field-aligned current strength and/or magnetospheric source plasma, or temporal evolution of the plasma along the flux tube, as suggested by McFadden et al. (1999). This type of structure is potentially a strong observational test on theories of generation of auroral acceleration potentials, and should be studied in more detail.

Perpendicular Spatial Scales One expects the perpendicular (to the geomagnetic field) scale sizes of the acceleration potentials to match those of the shortest dimension (typically north-south) of the optical discrete arcs. We are aware of no direct comparison of a quiet arc optical observation and a high-altitude electric field measurement giving the acceleration region scale size, but Figueiredo et al. (2005) report on conjugacy between Cluster measurements of the acceleration region at high altitude and optical observations of a dynamic horn arc associated with an auroral substorm-related surge. Many observations exist, however, relating optical arc widths to the resulting accelerated precipitation of electrons from the closure of these acceleration structure (e.g. Hallinan and Stenbaek-Nielsen 2001; Grubbs et al. 2018b).

A comparison between arc sizes and potential structures can instead be based on statistical investigations of potential scale sizes, but there are very few such studies. Johansson et al. (2007) gives scale sizes of converging electric field structures of 1–10 km with a median of 5 km (mapped to ionospheric altitude), based on 85 measurements. Care is needed in comparing this result with optical measurements, since the authors define scale size as the half width of the electric field structure, and not of the potential. It is therefore likely that their result is more applicable to the boundary of the U potentials, and not the whole potential structure (cf. Fig. 5). Similar sizes were reported by Hull et al. (2003b), with the same reservations. More statistical studies, with a view to compare with optical and low-altitude electron measurements are desirable.

Altitude Distribution Another important observational constraint for acceleration mechanisms is the altitude distribution of the acceleration potential. Several studies have addressed this by various methods (Fig. 9). Statistical investigations of the change of the perpendicular electric field with altitude has been used by Lindqvist and Marklund (1990) and Weimer and Gurnett (1993). The former study showed that the acceleration region extended to an altitude of 1.7 R_E, but did not give a clear lower limit, due to the limitations of the spacecraft orbit. Using DE1 data Weimer and Gurnett (1993) found that most of the potential drop was found below 1 R_E, but that a minor part of it extended up to 3 R_E. A similar study based on statistics of ion beam energies measured by Polar placed most of the potential drop between 1 and 2 R_E (Mozer and Hull 2001). The latter result is consistent with a recent study by Sadeghi and Emami (2019), who report that 30% of the potential drop is located between 0.9 and 1.2 R_E. In contrast, based on Cluster measurements on ion and electron beam energies, Alm et al. (2015) reported that 50% of the potential drop is located above 2 R_E with 20% remaining at an altitude of 3.4 R_E. Above 4.6 R_E the remaining parallel potential quickly drops to zero, perhaps indicating the presence of a high-altitude double layer (cf. Sect. 3.4).

Statistical studies of course include a wide variation in plasma properties along the flux tubes depending on e.g. season and geomagnetic activity. E.g. in a study based on Akebono data, Morooka and Mukai (2003) show that the altitude extent of the acceleration potential shifts to higher altitudes during winter. But such studies do not say much about instantaneous distribution of the potential drops. Information on the instantaneous distribution of the parallel potential drop can be estimated by some different techniques. Marghitu et al. (2006) and Forsyth et al. (2012) use a technique to determine the top of the acceleration region based on the anisotropy of the electron distributions. For both case studies, the top altitude varied considerably during passes of wide auroral structures (0.6–1.5 R_E and 1.6–2.8 R_E, respectively), indicating either large temporal or internal spatial variations.

Simultaneous spacecraft measurements at different altitudes of a stable potential structure have been used in a few recent studies. Marklund et al. (2011a) used two Cluster spacecraft passing the same acceleration structure (using combined particle and electric field measurements to verify that the total potential drop remained constant), and showed that for one acceleration structure the whole acceleration potential of 4 kV was located between 1 and 1.4 R_E. Using the same method, Sadeghi et al. (2011) concluded that 18% of the total potential drop was located between 1.13 and 1.3 R_E.

In order to make progress in constraining the parallel potential distribution, we suggest that systematic studies combining the techniques of Marklund et al. (2011a) and Marghitu et al. (2006) be performed.

Within the auroral acceleration region the ionospheric plasma that originally could be present on that field-line is expelled, together with part of the magnetospheric plasma. This results in the low-density region of the 'auroral cavity'. It has been proposed that the auroral cavity is well collocated with the acceleration region (e.g. Ergun et al. 2002b), while recent results indicate that it can extend to altitudes above the top of the acceleration region (Alm et al. 2015).

Potential Drop Verification that the electric potential structures are responsible for auroral acceleration can be carried out by combined particle and electric field measurements. The total parallel potential drop within a U-shaped potential structure located below a spacecraft can be determined by integration of the perpendicular electric field measured from a point outside of the structure to the centre of the structure. This potential drop should be the same as the energy of the ion beam if the potential structure below the spacecraft is static on the time scale of the ion transit time. The total acceleration potential is then obtained by adding

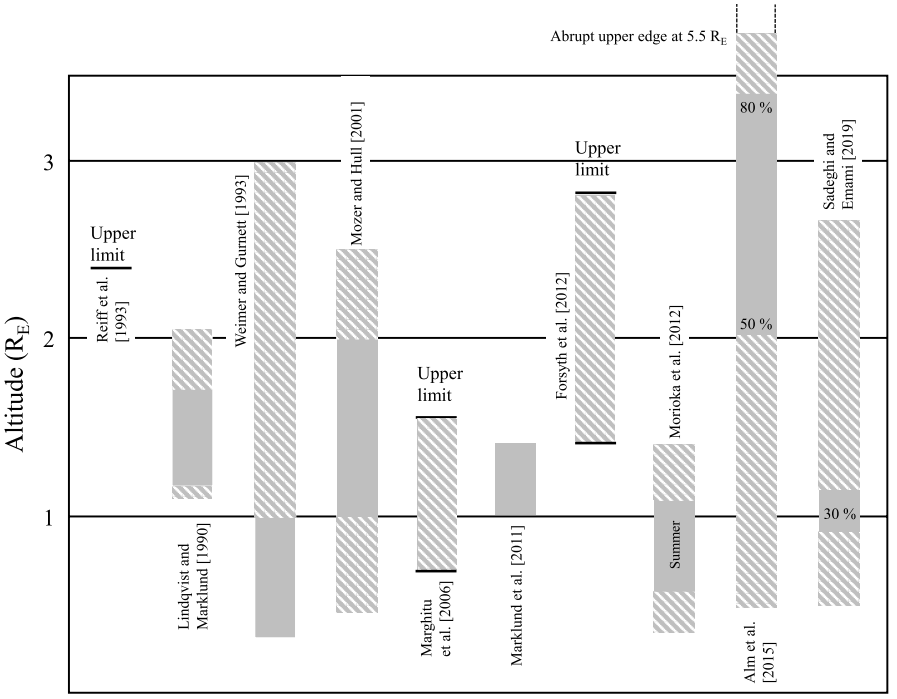

Fig. 9 Altitude distribution of the auroral acceleration region, reported by various authors. The hatched regions correspond to uncertain or varying results. Updated from Karlsson (2013)

the inferred acceleration potential of the electrons accelerated by the part of the potential structure extending above the spacecraft. Good agreement between ion beam energies and integrated electric potential drops was found using FAST measurements (McFadden et al. 1999), but there are few studies determining the total potential drop by this method. Case studies using Cluster passes through the acceleration region (additionally showing that the total potential drop stays constant on time scales similar to the satellite separation time) give expected potential drops of 4–7 kV (Marklund et al. 2011a), 3–3.3 kV (Sadeghi et al. 2011), 4.2–17.7 kV (Alm et al. 2013) (excluding a dayside event), and 2 kV (Forsyth et al. 2012). However, comprehensive statistical studies are missing.

Direct Measurements of $E_\parallel$ Direct observation of the parallel electric field $E_\parallel$ within the acceleration region by conventional double probe techniques is problematic due to several technical limitations, such as spacecraft shadowing of particle fluxes and asymmetric work functions of the probes (e.g. Karlsson 2012). However, when the parallel electric fields are large enough, detection may be possible. Mozer and Kletzing (1998) and Hull et al. (2003a) used the three-axis electric field measurements of the Polar satellite to demonstrate the likely existence of upward-directed parallel electric fields of a magnitude of 200–300 mV/m at an altitude of around 1 R_E. Ergun et al. (2002a) reported on a large number of FAST observations of upward-directed parallel electric fields in the form of strong, oblique double layers at the lower boundary of the auroral cavity. They concluded that these double layers contributed 10–50% of the total potential drop. There is also some evidence for the existence of double layers at somewhat higher altitudes, inside the auroral cavity (Ergun et al. 2004) (see

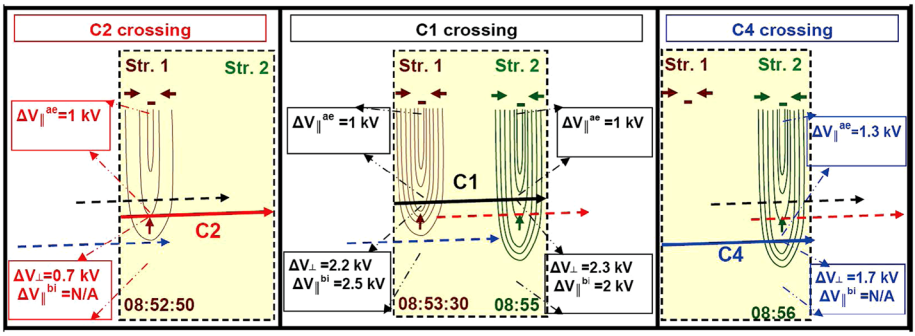

Fig. 10 Schematic of temporal evolution of two acceleration potentials based on measurements from Cluster 1, 2, and 4 (Sadeghi et al. 2011). The boxes below the spacecraft paths show the potentials below the spacecraft orbits, inferred from the electric potential drop and from the characteristic energy of the upgoing ions, while the boxes above the paths show the potential above the spacecraft, based on the energy of downgoing electrons. The crossing times of the structures are indicated at the bottom of the figure

also Fig. 5). For a more detailed discussion of double layers in the auroral region, see also Andersson and Ergun (2012).

Time Scales While a defining characteristic of the quiet arc is its relative temporal stability (cf. Sect. 2), the potential structures do change with time. The life time, and typical time scales for changes in the potential drop, size and location of the acceleration structures are important observational constraints to models of such structures. It is a striking fact that optical observations of quiet arcs show that their lifetimes can be tens of minutes (Knudsen et al. 2001), or even several hours (Galperin 2002). For acceleration structures, again, there exist no large statistical study, but a number of case studies based on multi-spacecraft observations exist.

Cluster multi-spacecraft observations show that acceleration structures can keep a clearly identifiable identity during up to 50 min (Figueiredo et al. 2005), and have very little change in total potential drop and width for around 5 minutes at an altitude of 1 R_E (Marklund et al. 2011a). Sadeghi et al. (2011) show, on the other hand, that an acceleration structure (structure 1 in Fig. 10) increased its potential drop significantly (from 1.7 kV to 3.5 kV) during 40 s. Interestingly, this increase took place exclusively below 1.3 R_E, while the potential drop stayed constant at 1 kV above this altitude. A similar result was reported by Forsyth et al. (2012) with an increase of the acceleration potential of 2 kV below an altitude of 4600 km during 150 s, while the potential above this altitude remained unchanged. While the field-aligned current density increased during this event, it remained constant in the Sadeghi et al. (2011) event, indicating changing plasma properties on the field line, as suggested by McFadden et al. (1999) in the context of auroral fingers.

While the study of temporal properties based on direct measurements of the electric potential structure is based on few cases, there is some supporting statistical studies of the resulting downward accelerated electrons. In an early small statistical study by Thieman and Hoffman (1985), the DE satellites were used to study the temporal stability of inverted-V electron precipitation. They concluded that well-identifiable inverted-V events could have life times of at least 18 minutes, and that the growth and decay of the events had similar time scales. A larger study by Boudouridis and Spence (2007), using two DMSP satellites showed that electron precipitation structures have a high correlation between the spacecraft up until around 2 min for scales sizes of 50–100 km, with lower correlation times for smaller scales.

More recently two studies have investigated the temporal stability of field-aligned currents, using the ST5 satellites. Gjerloev et al. (2011) reports that field-aligned currents with scale-sizes greater than 200 km (mapped to ionospheric altitudes) have life times of the order of a minute, consistent with the result of a smaller study by Le et al. (2009). The somewhat disparate results of these studies, as well as the unclear exact relation to discrete auroral arcs means that there is a need for more detailed statistical studies of temporal properties of structures clearly identified with discrete arcs.

When interpreting results on life times of aurora accelerations structures, as well as of optical signature of arcs, one must keep in mind that there is a certain uncertainty in its definition. A concept such as 'clearly identifiable identity' is somewhat vague and can be interpreted in different ways by different authors.

3.5 The Return Current Region

As mentioned in Sect. 3.3, the upward current region is often associated with a region of downward or 'return' current. Originally this region was thought to be a passive region, where the current was simply carried by thermal ionospheric electrons. The first indication that the situation was more complicated came from early observations of upward-directed strongly field-aligned fluxes of electrons accelerated up to energies of 500 eV (Klumpar and Heikkila 1982), as well as observations of extremely large, diverging electric fields at low altitudes (1400–1800 km) (Marklund et al. 1994; Karlsson and Marklund 1996).

Measurements from the FAST satellite greatly increased the observational knowledge of the return current region. Results from earlier than 2002 are covered in detail in the ISSI Auroral Plasma Physics book (Paschmann et al. 2003); we will here give a short recapitulation and update. Figure 6 shows a typical return current region from approximately 16:47:30 UT to 16:48 UT. The downward current (consistent with the gradient of the magnetic field) is carried by upgoing electrons with energies up to the order of 1 keV (Carlson et al. 1998b; Elphic et al. 1998). These electrons have a very low perpendicular temperature, which indicates their ionospheric origin (Carlson et al. 1998b). The integrated potential of the diverging electric fields collocated with the beams typically matches the beam maximum energy, which is strong evidence that the beam electrons have been accelerated by a quasi-static parallel electric field. However not all beams show a good correlation with the electric potential (Andersson and Ergun 2006), which may indicate acceleration by dynamic processes, e.g. Alfvén waves or evolving electric fields (Marklund et al. 2001; Andersson et al. 2008). Direct measurements of the parallel electric field have shown that it often takes the form of double layers with a parallel thickness of a few Debye lengths, moving upward along the field line approximately at the ion acoustic velocity (Andersson et al. 2002; Ergun et al. 2003).

The electron beam is strongly thermalized (Carlson et al. 1998b; Andersson and Ergun 2012), with a temperature comparable to the beam energy, which leads to a counter-streaming tail of the electron distribution. This thermalization is very likely connected to the presence of strong broadband electrostatic low frequency (BBELF) turbulence (e.g. Shen et al. 2018; Lynch et al. 2002), although the causal relation is not clear. The electron beams have at times been observed all the way up to an altitude of 3–4 R_E (Wright et al. 2008). At the low altitude end, sounding rocket observations in the F-region nightside often observe sharply localized return current signatures in magnetic field data, immediately adjacent to discrete arcs and tightly coupled to DC electric field structures (Lynch et al. 2015; Zettergren et al. 2014; Clayton et al. 2019b). As discussed in the next section, the horizontal current closure between adjacent upward and downward field aligned current structures demonstrates interesting ionospheric physics.

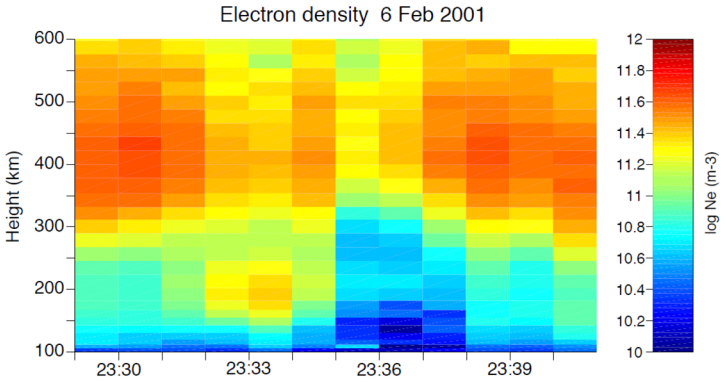

Fig. 11 EISCAT observations of ionospheric plasma densities, with a deep cavity (23:35 UT to 23:38 UT) in the downward current region. Adapted from Aikio et al. (2004)

The intense BBELF wave activity is believed to result in perpendicular heating of the ions in the return current region, which due to the conservation of the magnetic moment produces ion conics at higher altitudes (Carlson et al. 1998b; Lund et al. 1999; Lynch et al. 2002). Thus there is a considerable outflow of ions from the ionosphere in the return current region, something that considerably changes the plasma environment in the region.

Ions are also moving downwards in the form of accelerated beams (Andersson et al. 2002; Cattell et al. 2002; Hultqvist 2002), oppositely to the situation in the upward current region. However the combination of downward acceleration of ions and ion heating due the waves result in a 'pressure cooker' effect, and together with the requirement for the double layer to be in pressure balance, results in an anti-earthward motion of the double layer. The result is an efficient process to remove ions from the ionosphere (Hwang et al. 2008).

This asymmetry with the upward current region also extends to optical emissions; the return current region often is associated with the 'black aurora' (e.g. Trondsen and Cogger 1997; Peticolas et al. 2002), which are well-delimited regions of a lack of auroral emissions both of the diffuse and accelerated types. Both the ion beams and the lack of auroral emissions are consistent with a region of downward-directed $E_{\parallel}$, which can both accelerate ions downwards, and block access to the atmosphere and ionosphere for plasma sheet electrons (Archer et al. 2011). On the other hand, it has been suggested that rather than the electrons being blocked from access by en electric field, some magnetospheric mechanism may suppress the scattering of electrons into the loss cone in the first place (Peticolas et al. 2002; Blixt et al. 2005; Gustavsson et al. 2008; Obuchi et al. 2011; Sakanoi et al. 2012). This second type of black aurora probably takes place in the diffuse auroral region, and is not necessarily associated with a return current region. Similarly to the ordinary aurora, the black aurora exhibits not only elongated arcs, but also other types of geometrical shapes (Trondsen and Cogger 1997; Kimball and Hallinan 1998; Obuchi et al. 2011; Sakanoi et al. 2012), something that for the reurn current black aurora seems to also be reflected in variations in the shape of the electric field acceleration structures (Hwang et al. 2006a,b; Johansson et al. 2006).

An important consequence of the return current is the creation of deep density cavities in the E and F regions, created by a plasma outflow and increased recombination in the regions where the downward current closes to perpendicular currents (Doe et al. 1993, 1994; Aikio et al. 2004; Zettergren et al. 2014). Simulations by Zettergren and Semeter (2012), Karlsson et al. (2005) show that the depletion of E-region plasma occurs on a fast time-scale of 5–30 s

depending on the current-system scale size. In the F-region, enhanced recombination from conversion of the plasma to molecular ions, a comparatively slower process (120–300 s), contributed to the depletion. The resulting low plasma densities and associated low conductivities may provide an important feedback to the magnetosphere (e.g. Karlsson et al. 2007). These structures are further discussed in the companion paper by Lysak et al.

4 Horizontal Dynamics, Ionospheric Current Continuity

A key element for auroral electrodynamics is the electric field, **E**, driven by magnetospheric convection and mapped to ionospheric altitudes along magnetic field lines. The ionospheric electric field differs from the magnetospheric electric field by the potential drop in the auroral acceleration region; it can also be a source/driver through local polarization charges and flows. Altogether, the electric field distribution and ionospheric convection are related to each other via the frozen-in condition, where $\mathbf{E} = -\mathbf{v} \times \mathbf{B}$ (down to the F-region), and thus flow fields around aurora, as read, e.g., by motion of visible structures and boundaries in TV images, can include information on the electric field structure. At the same time, the electric field and the ionospheric current, (which can be determined via Ohm's law, once the ionospheric conductance is known), are coupled through the continuity equation. The current system of the auroral arc, governed by ionospheric closure of the field-aligned current and Ohm's law, is summarized under Sect. 4.2.

4.1 Horizontal Dynamics

Studies of the auroral zone as seen by conjugate observations of SuperDarn and auroral imagery set the stage for a discussion of the horizontal dynamics of auroral activity. Zou et al. (2012, 2009a) and Bristow et al. (2003) show examples following the evolution of substorms and westward surges, showing the relationship between flow structures seen by the radars, and the motion of the arc systems as the oval evolves. Flows move around arcs and around the Harang discontinuity, and the oval itself moves equatorward and poleward, as the auroral system responds to the reconfiguration of current structures. The relationship between the flow structures and the visible signatures depends on the morphology: activity, local time, magnetic latitude, and sequence of events. More local studies using PFISR or EISCAT together with auroral imagery (Nishimura et al. 2014; Aikio et al. 2002; Semeter et al. 2010) explore the local signatures of flows near auroral arcs during the growth phase of substorms; the even more local studies of Archer et al. (2017) and Clayton et al. (2019b) show the finely detailed relationships between these features illustrated by conjunctions between in situ field observations and ground imagery. In all these cases, the underlying physics relating the auroral brightness—the precipitating energetic electrons—to the flows—the ionospheric DC electric field—is governed by the current continuity equation, as we discuss below.

Historically, explorations of the physics of these current continuity rules have focussed on idealized sheetlike arcs, with limited to no variation along the length of the arc. While sheetlike arcs—quiet discrete arcs, as the topic of this chapter—form a large portion of auroral signatures, their evolution and variability is of great interest; and, fully understanding the three dimensional structure of a simple sheetlike arc is critical for moving on to more complex situations. Three dimensional time dependent ionospheric models such as GEMINI (Zettergren and Semeter 2012; Zettergren and Snively 2015, 2019; Zettergren et al. 2015) and GITM (Ridley et al. 2006) allow us to explore these relationships in more complicated

environments. Below we begin with the idealized arc and work through the implications of current continuity for increasingly complex morphologies. Even simple sheetlike arcs have interesting volumetric conductivity behaviour, from which much can be learned.

4.2 Ionospheric Current Continuity

The ionospheric closure of the field-aligned current can be addressed starting from the (quasi-)steady form of the current continuity equation, $\nabla \cdot \mathbf{J} = 0$, where time variation of the charge density is neglected. In a reference system where the field-aligned current, $j_\parallel$, is assumed perpendicular to ionosphere (roughly true in the auroral region), current continuity and Ohm's law can be worked out to

$$j_\parallel = \nabla \cdot \mathbf{J}_P + \nabla \cdot \mathbf{J}_H = \Sigma_P \nabla \cdot \mathbf{E} + \nabla \Sigma_P \cdot \mathbf{E} - (\nabla \Sigma_H \times \mathbf{E})_\parallel - \Sigma_H (\nabla \times \mathbf{E}))_\parallel \quad (2)$$

where it is also assumed that magnetic field lines are equipotential and, consequently, the electric field, $\mathbf{E}$, is constant and maps through the F and E regions. Ionospheric Pedersen and Hall conductivities and currents can be integrated across the ionospheric height to the conductances Σ_P, Σ_H, and the currents $\mathbf{J}_P$, $\mathbf{J}_H$, respectively. The ionosphere is thus represented as a boundary layer and the divergence operators of the continuity equation operate in the 2-D plane of this layer. Nonetheless, the thick uniform arc model below takes into account also the thickness of the ionosphere; and, various altitudinally striated ionospheric models exist and are used for different studies (Lysak 1999; Ridley et al. 2006; Zettergren and Semeter 2012).

Even with an altitude-striated picture, the cumulative effect from height integrated conductances in the continuity equation still provides a valuable summary of the system. Equation (2) is written in the system of the neutral atmosphere, whose motion (the neutral wind) is often neglected, because it is rarely available, and the equivalent electric field is typically small compared to auroral electric fields. However, this is not always true, and a comprehensive examination of the neutral wind influence on auroral electrodynamics is yet to be performed. One nightside case study event of a discrete arc (from a sounding rocket event) explored, among other things, the effects of neutral winds using the GEMINI model (Lynch et al. 2015; Zettergren et al. 2014), showing the range of possible neutral wind effects on the terms of the continuity equation; for that event the effects could reach 10% depending on whether the neutral winds were sympathetic with the plasma motion.

Equation (2) is independent of the geometry of aurora and in general used by neglecting the inductive last term. While the last term is indeed negligible under (quasi-)steady conditions, it becomes important e.g. during substorms, when it accounts (Yoshikawa 2002b,a) for the inductive rise (and fall) of the divergence free part of the ionospheric current (not coupled to field-aligned current).

The geometry-independent form of current continuity and Ohm's law underlies a broad range of auroral studies, most of them based on ground observations (like magnetic field and optical data), addressing 2-D auroral features on meso- to large scale (see, e.g., the review by Vanhamäki and Amm 2011). More recently, 2-D investigations became possible also on small scale, by experiments like Auroral Structure and Kinetics (ASK, e.g., Lanchester and Gustavsson 2012). Next we explore more closely just the particular subset of elongated auroral forms, also known as auroral arcs, where the 2-D description can be further adapted to the (quasi)1-D arc geometry, with gradients (much) steeper across the arc than along the arc.

Equation (3) is adapted for this arc geometry, with ξ the direction across the arc (typically close to geomagnetic northward) and η the direction along the arc (typically close to geomagnetic eastward).

$$j_{\parallel} = \Sigma_P \frac{\partial \mathbf{E}_{\xi}}{\partial \xi} + \frac{\partial \Sigma_P}{\partial \xi}\mathbf{E}_{\xi} + \Sigma_P \frac{\partial \mathbf{E}_{\eta}}{\partial \eta} + \frac{\partial \Sigma_P}{\partial \eta}\mathbf{E}_{\eta} + \frac{\partial \Sigma_H}{\partial \eta}\mathbf{E}_{\xi} - \frac{\partial \Sigma_H}{\partial \xi}\mathbf{E}_{\eta} \tag{3}$$

The various terms on the right hand side are colored in blue (terms 1, 2), red (terms 3, 4, 5), or green (term 6), according to the related arc model, indicated with the same color at the top of Fig. 12. Thus, the blue terms are related to the thin uniform 1-D arc model, where the ionospheric thickness and gradients along the arc are neglected. The red terms are related to the thin non-uniform 2-D arc model, where ionospheric thickness is again neglected but gradients along the arc are allowed, even though the 1-D backbone is preserved. Finally, the green term is related to the Cowling effect (Cowling 1932; Chapman 1956), that can be understood by a thick uniform 2-D arc model, where the thickness of the ionosphere is no longer neglected, but gradients along the arc are ignored. Specific features of these three arc models are summarized below, following the review by Marghitu (2012).

In the case of the thin uniform 1-D arc, the field-aligned current is closed in the ionosphere by Pedersen current, driven by an electric field normal to the arc, while the Hall current electrojet (EJ) along the arc, driven by the same electric field, is divergence free. The 1-D symmetry is often extended to oval scales (e.g., Sugiura 1984), where gradients in the meridional direction dominate, under steady state, over gradients in the azimuthal direction.

Despite the seeming simplicity of the 1-D model, radar, rocket, and satellite observations exhibit a broad range of electric field profiles around the arc, addressed systematically by Marklund (1984) and shown to depend on the relative contributions to current closure by ionospheric polarization and field-aligned current. Subsequently, Chap. 6 of the ISSI book on Auroral Plasma Physics (Paschmann et al. 2003), included a follow-on examination of the electric field pattern around the arc, depending on the orientation of the background electric field with respect to the arc, under negligible (Fig. 6.2) and significant (Fig. 6.5) field-aligned current. In terms of (3), the field-aligned current above the arc (l.h.s. term) induces the enhanced conductance slab. This, in turn, is responsible for the current driven across the arc by the polarization electric field (first l.h.s term), generated by polarization charges accumulated at the arc edges. It also results in the current at these arc edges (second l.h.s. term), where the Pedersen conductance varies sharply. While these three terms balance each other under 1-D geometry, the field-aligned current on the l.h.s. is often small compared to the ionospheric current on the r.h.s.

Note the inherent limitation of this 'discrete' explanation of a continuous mechanism, explored further below in relation to Cowling channel, under the thick uniform 2-D arc model. Note as well that the relative weight of polarization and field-aligned current in providing ionospheric current continuity depends largely on the magnetospheric end of the auroral current circuit, whose structure is in general unknown, though the driving FAC can be measured. One cannot fully resolve the ionospheric end independent of the rest of the circuit, but a full picture of the ionospheric footpoint including its horizontally distributed current closure, as represented by (3), can be constraining. Recent advances in filtered groundbased imagery add data to this question, as the filtered imagery can provide 2D+time estimates of precipitating energy flux and characteristic energy, constraining possible magnetospheric sources (Grubbs et al. 2018; Clayton et al. 2019b). In situ observations of precipitation and fields have been used to infer magnetospheric drivers such as U-shaped potential structures (Hallinan et al. 2001).

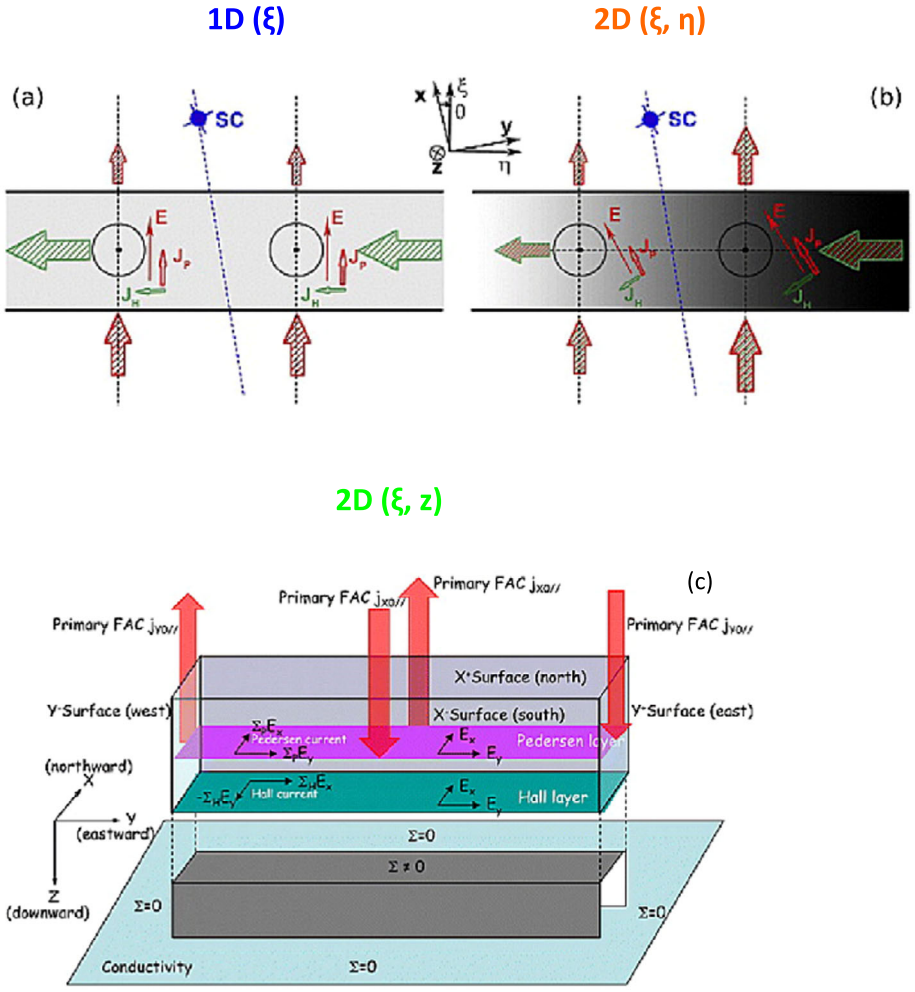

Fig. 12 (**a**) Thin uniform, (**b**) thin nonuniform, and (**c**) thick uniform (Cowling channel) arc models. Compound figure from Marghitu (2012), with panels (a) and (b) from Marghitu et al. (2011), and panel (c) from Fujii et al. (2011). In panels (**a**) and (**b**), the conductance, field-aligned current (FAC), ionospheric electric field, and ionospheric current are indicated by the gray shade, circles, solid arrows, and hatched arrows, respectively. Red and green arrows show the Pedersen and Hall components of the current. For simplicity, the conductance variation in normal direction is not shown (but is taken into account in the text). Note that in panels (**a**) and (**b**) the (ξ, η) frame is associated with the arc and (x, y) with the satellite overpass, while in panel (**c**), the (x, y) frame is associated with the arc. For consistency, x is replaced by ξ in the panel title

The use of a three-dimensional ionospheric model such as Gemini can help illustrate these relationships. An example is shown in Fig. 13, based on observations from PFISR and from filtered groundbased imagery of a quiet premidnight sheetlike arc over Poker Flat in winter 2017.

The case of thin non-uniform 2-D arc was substantiated by event studies of Marghitu et al. (2004, 2009, 2011), based on data observed by the FAST satellite (Carlson et al. 1998a). Data analysis by the newly introduced AuroraL Arc electroDYNamics (ALADYN) technique indicated that the electrojet divergence was significant at certain locations and,

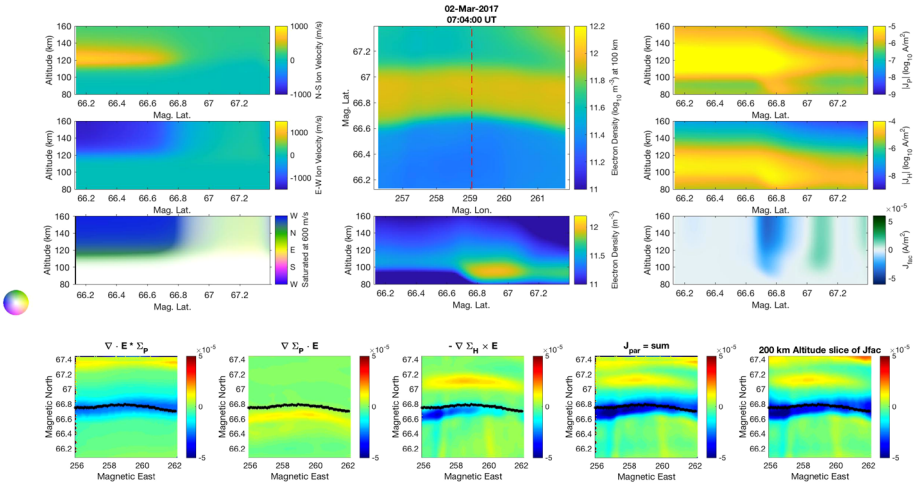

Fig. 13 Examples of GEMINI model output representing an event from the winter 2018 Poker Flat rocket campaign, as seen by PFISR and filtered groundbased imagery. The model is driven by precipitation maps created from the filtered imagery, and by two-dimensional electric field maps created by replicating the PFISR vvels (vector velocities) line of vectors along the extent of a sheetlike arc structure. The first set of panels show various cuts of flows, density, and current through the 3d modelled volume. The bottom set of panels show the pieces of (2) (Clayton et al. 2019a)

moreover, comparable to the FAC (field-aligned current) density, suggesting FAC closure also along the arc, by coupling to the electrojet. More recently, a statistical study by Jiang et al. (2015b), based on 181 growth phase arcs observed by FAST, provided further evidence for FAC–EJ coupling, by showing that the Pedersen current supposed to close the FAC across the arc is equal, on average, to just half of the field-aligned current (see Fig. 11 of this study). While the authors attributed the mismatch to underestimation of the ionospheric conductance, FAC–EJ coupling may play a role too.

Longitudinal gradients can become significant during the substorm growth phase, when the upcoming 1-D break-up arc 'prepares' to transform into 2-D aurora, and comparable to the meridional gradients at the substorm onset, when 1-D symmetry is lost. The mismatch found by Jiang et al. (2015b) can be regarded as a quantitative confirmation of this qualitative perspective, though a detailed examination of the data has not been performed so far.

The ALADYN technique can provide a local estimate of the electrojet divergence based on single-spacecraft data, but cannot indicate the respective weights of the longitudinal gradients in conductance and electric field (the red terms in (3)). In order to achieve such a goal, at least two satellites are needed, to sample the data at different locations along the auroral arc or oval, separated by a distance comparable to the electrojet length scale. Such a configuration is provided by the Swarm mission (Friis-Christensen et al. 2008), launched in November 2013. However, since precipitating particles are not directly measured, conductance proxies (e.g., like those of Robinson et al. (1987)) are more difficult to derive and the examination of the FAC closure in the longitudinal direction is yet to be done. Recent work however using imagery such as the THEMIS and REGO GBO databases (Mende 2008) can provide the necessary 2D+time context. An example case study is provided by the Isinglass sounding rocket study (Clayton et al. 2019b), where in situ flow data (along a rocket trajectory) is combined with ground imagery to replicate the trajectory at a variety of crossing

points along the longitudinally-extended arc, in order to create a 2D flow field for driving the GEMINI model.

Until such a study is performed, a model based on a uniform FAC sheet and an electrojet divergence dominated by longitudinal gradients in conductance was suggested by Marghitu et al. (2009) (see in particular their Fig. 11), with the upward FAC above the arc fed by an electrojet of decreasing intensity—associated with decreasing conductance, related in turn to decreasing electron energy. The FAC can couple mainly to the Hall component of the electrojet for electron energies above some 5 keV, specific to active aurora, while coupling to both Pedersen and Hall component is possible at lower energies, as observed for quiet arcs. The model was further explored by Marghitu et al. (2011), who looked also at the direction across the arc, in the limit of low polarization. In this limit, supported for quiet aurora by the study of Amm et al. (2011), the results were found to be consistent with a divergence free Hall current, appropriate for quiet aurora. Moreover, (vanishingly) small tangential electric fields were found to characterize long arcs (as expected from the 1-D model), whereas substantial tangential electric fields, as observed, e.g., in the Harang region, were related to a higher probability of FAC coupling to Hall current, likely to happen during active times—in agreement with the dynamic character of the Harang region (Zou et al. 2009b). Many of these permutations can be explored with 3D ionospheric models such as GITM (Ridley et al. 2006) and GEMINI (Zettergren and Snively 2019). These models allow cuts along and across arc structures to illustrate how the different terms of the continuity equation interact, as illustrated in Fig. 13.

The thick uniform 2-D arc follows the Cowling channel model suggested by Amm et al. (2011) and Fujii et al. (2011), who addressed the competing contributions of polarization and FAC to ionospheric current continuity from a novel perspective. The textbook description of the Cowling channel emphasizes the multiplication effect on conductance and current along the channel, in a 1-D geometry: the primary electric field along the channel drives both a primary Pedersen current along the channel and a Hall current across the channel, which results in polarization charges at the channel boundaries (typically sharp gradients in conductance). The polarization electric field drives a secondary Pedersen current across the channel and a secondary Hall current along the channel, that adds to the primary Pedersen current and provides the multiplication effect, which scales with $(\Sigma_H/\Sigma_P)^2$. For a conductance ratio of around 3, which is large, but not unusual for active events, the current along the channel can be multiplied by one order of magnitude.

For simplicity, the textbook description concentrates on polarization and neglects the role of the FAC, that can discharge part of the polarization and reduce thus the multiplication effect. The result is a partial Cowling channel and relevant arc observations were discussed, e.g., in the review by Marklund (1984). More recently, Amm et al. (2011) formalized the efficiency of the Cowling effect, equivalent to the 'completeness' of the Cowling channel, in differential, geometry independent form, by a parameter C, with values between 0 and 1, indicating what fraction of the Hall current divergence is closed by the divergence of the polarization Pedersen current,

$$\nabla \cdot \mathbf{J}'_P = -C \nabla \cdot \mathbf{J}_H. \tag{4}$$

An efficiency of 1, equivalent to the complete Cowling channel, implies no FAC discharge of the polarization built up by the primary Hall current, while efficiency 0 is equivalent to no Cowling channel and full coupling of the Hall current For a 1D Cowling channel, the divergence of the Hall current reduces to the last (green) term in (3), while the divergence of the polarization Pedersen current is a fraction of the divergence of the total Pedersen cur-

rent (the two blue terms), which includes also the primary Pedersen current, driven by the primary electric field, of magnetospheric origin. As noted already with respect to the 1D model, the weight of the polarization Pedersen current in the total Pedersen current, equivalent to knowing C, or the capability of the Hall current to build up polarization charges, (and not fully discharged via field-aligned currents), cannot be derived by just looking at the ionospheric end of the current circuit. Still, by analyzing electrojet data from ground magnetometers and radars, Amm et al. (2011) were also able to show that the probability of a high Cowling efficiency scales with geomagnetic activity.

In a companion paper, Fujii et al. (2011) advanced the Cowling channel model by giving up the approximation of a thin ionosphere and taking into account the different altitudinal profiles of the Pedersen and Hall conductivities (see Fig. 13 for an example of these altitudinal profiles.) Consequently, they suggested a model with Pedersen and Hall layers at different altitudes, as indicated in panel (c) of Fig. 12. The Hall current, at lower altitude, couples to FAC between the two layers, then part of it connects to the secondary Pedersen current, driven by the polarization electric field, while the other part escapes to magnetosphere. The Cowling channel is complete when the ionospheric loop of the Hall, FAC, and Pedersen current has no FAC leakage to the magnetosphere.

Fujii et al. (2011) gave up not only the thin ionosphere, but also the infinite longitudinal extension of the Cowling channel, assuming boundaries both across and along the channel, visible as well in panel (c) of Fig. 12. This has the important consequence that polarization charges can build up at the longitudinal ends of the channel, driving a polarization electric field also along the channel, though in other respects the channel remains uniform. Later on, Fujii et al. (2012) used the model to explain the equatorward motion of an afternoon arc, together with its current system, driven self-consistently by the polarization electric field along the Cowling channel associated with the arc. While the need for a height resolved ionosphere, in particular with respect to MIT coupling, has been identified for quite some time (e.g., Amm et al. 2008), studies like those mentioned above remain scarce, and likewise underlying in-situ observations. This may change in the future, e.g., if mission proposals like Daedalus (Sarris et al. 2019), recently selected by ESA for a detailed feasibility study, will materialize, and simultaneous ionospheric samplings at different altitudes will become available systematically.

An interesting problem raised by the Cowling channel model outlined above is related to the apparently increased likelihood that Cowling efficiency is high when geomagnetic activity is high, noticed by Amm et al. (2011). A (quasi) complete Cowling channel implies significant energy dissipation, via the secondary Pedersen current; but on the other hand the missing FAC connection to the magnetosphere raises the issue of missing energy input, typically delivered as Poynting flux, via the FAC system of the channel. This problem cannot be solved under steady state conditions and requires a time dependent framework, where energy delivery and energy dissipation are not necessarily simultaneous (and collocated). Such a formal framework was introduced by Yoshikawa et al. (2013) and checked on a numerical test case by Yoshikawa et al. (2013). A comprehensive review of recent Cowling channel developments, including those outlined above, is available in Yoshikawa and Fujii (2018).

To conclude this section and try to look a bit into the future, it seems clear that a complete understanding of the auroral arc current system requires a 3-D model, ideally time dependent, where length, width, and thickness are all taken into account. Recent work such as illustrated in Fig. 13 is helping to visualize this region. The 1-D backbone may still help to formalize such a model in a relatively simple framework, as yet not available, perhaps even tractable analytically. Future multi-point observations of the 3-D arc may help as well to un-

ravel its structure. While radar, rocket, and single satellite observations were and still are the main tool for arc exploration, typically along a 1-D cross-section of the arc, this paradigm may change in the (near?) future, by easy access to space of CubeSat fleets—as planned, or already under development, by various research groups around the world. Upcoming ground facilities, like EISCAT 3D, may also shed new light on the complexity of aurora, including the 'simple' auroral arc.

5 Single and Multiple Arcs

Instead of a single narrow structure, auroral arcs often appear in multiple sets (Stenbaek-Nielsen et al. 1998), making up the bulk of discrete auroral observations (Gillies et al. 2014). A quasi-static multiple arc system in the nightside auroral oval consists of 2–5 discrete forms, aligned in the east-west direction and nearly parallel to each other. The latitudinal width of individual arcs is about 10–20 km (Sesiano and Cloutier 1976; Akasofu et al. 1966; Vondrak et al. 1983; Knudsen et al. 2001; Wu et al. 2017). A common separation distance between two adjacent arcs is between 30–50 km, and there are some arcs separated by more than 100 km. The orientation of arcs in multiple arc systems is similar to that seen for single arcs, including a small deviation from lines of constant geomagnetic latitude that reverse signs near midnight (Gillies et al. 2014). The multiple structures can occur during both quiet and active periods. However, they are more nearly parallel to each other and more easily identified during less active times, typically associated with slow equatorward motion of the aurora (Akasofu et al. 1966, 1967). Field-line resonance (FLR) arcs also display multiple structures, but with a temporally periodic morphology and poleward motion (Gillies et al. 2018).

The field-aligned current (FAC) system associated with multiple auroral arcs has attracted much attention in both satellite and rocket studies (e.g. Armstrong et al. 1975; Sesiano and Cloutier 1976; Kamide and Akasofu 1976; Aikio et al. 2002; Juusola et al. 2016a). Stenbaek-Nielsen et al. (1998) reported multiple arcs observed both by an aircraft-borne all-sky camera and from electron energy spectrometers on FAST. The arcs are found to be associated with upward field-aligned current, as described in Sect. 3.3, and are identified by multiple peaks in energy and flux spectra of down-going electrons (inverted-V events). However, the relation between arcs and current sheets is not one-to-one, since an arc indicates an enhancement in electron energy flux but not necessarily in upward field-aligned current. Wu et al. (2017) investigate the large-scale FACs observed by the Swarm satellites and show the 'unipolar' and 'multipolar' FACs associated with multiple arc systems. In 'unipolar' FAC events, each arc is an intensification within a broad, unipolar current sheet and downward return currents occur outside of this broad sheet (Fig. 14). In 'multipolar' FAC events, multiple arc systems represent a collection of multiple up and down current pairs. They also found 'unipolar' FAC pattern is more common for quasi-static multiple arcs in the pre-midnight, pre-substorm auroral zone.

Of smaller width than the above meso-scale arc set is the multiple arc system composed of elements each having a width of the order of several hundred meters (Maggs and Davis 1968; Davis 1978; Borovsky 1993; Trondsen and Cogger 1997). Such an array of arcs can appear in diffuse aurora (Stenbaek-Nielsen et al. 1998) or blend together to give the impression of one single arc when not viewed in the magnetic zenith. When the system is active,

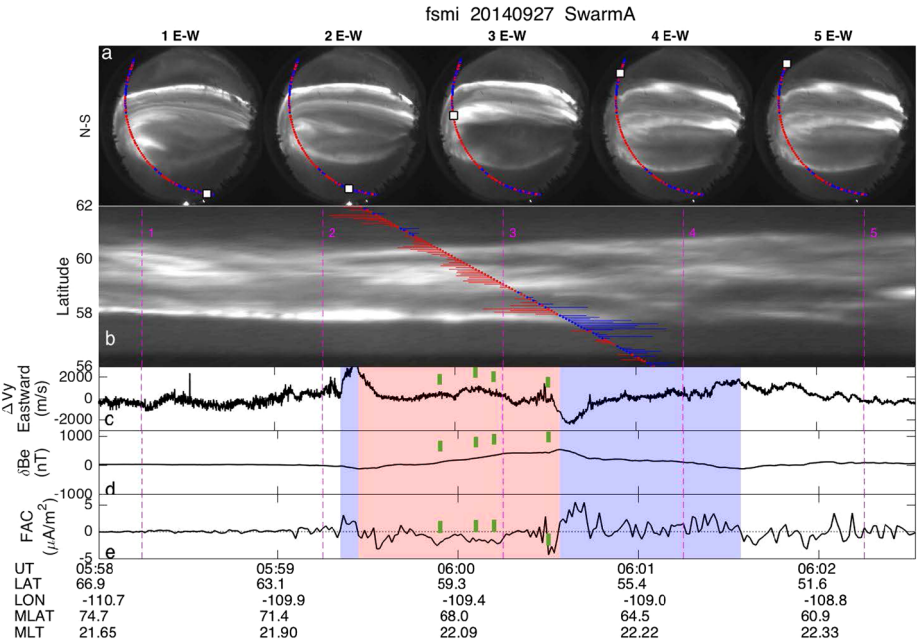

Fig. 14 Multiple arcs observed by the Fort Smith ASI and Swarm A with a "unipolar" FAC system. (**a**) The Swarm A trajectory and multiple arcs in the ASI images at 1-minute time intervals. Red and blue colors indicate upward and downward FACs. (**b**) Satellite-aligned keogram of Swarm A as a function of geomagnetic latitude and time. The values of upward (red) and downward (blue) FACs are displayed together with the flight path. (**c**) Horizontal cross-track (approximately eastward) ion velocity in m/s. (**d**) Eastward component of residual magnetic field. (**e**) Field-aligned current density $j_{\parallel}$ ($\mu A/m^2$) derived from the single satellite method. The red and blue areas in panels (**c**)–(**e**) are large-scale upward and downward FAC regions identified interactively by neglecting small-scale fluctuations. The positions of peak brightness of arcs are indicated by green lines (Wu et al. 2017)

motions along individual arcs frequently occur, and it is common to see opposite directions of motion along adjacent arcs (Hallinan and Davis 1970; Trondsen and Cogger 1997; Vogt et al. 1999b; Miles et al. 2018).

Multiple arcs are also a common feature in the dayside auroral oval, especially in the local time sector between 14 and 16 hours (Lundin and Evans 1985; Meng and Lundin 1986; Elphinstone et al. 1996; Sandholt et al. 2006). The precipitating electrons with energies of 0.3-2 keV in this local time sector usually appear as multiple narrow structures in latitude (Evans 1985). Moen et al. (1994) showed examples of postnoon discrete arcs with a thickness of 10-20 km and a lifetime of about 2 to 5 min. Kozlovsky et al. (2009) demonstrates these arcs were located in the region of the postnoon convection reversal, and the background upward FAC had a density of about 1 $\mu A/m^2$.

One interesting question about multiple arc systems is the source of multiplicity. Currently proposed theories include a structured magnetospheric generator (Akasofu and Chapman 1961; Coppi et al. 1966), instability in the ionosphere (Atkinson 1970), multiple reflection of Alfvén waves (e.g. Maltsev et al. 1977; Mallinckrodt and Carlson 1978; Haerendel 1994; Lysak 1990) and the internal structuring of the M-I coupling medium (stationary inertial Alfvén waves) (Knudsen 1996). The observations discussed in this section are meant to provide constraints for candidate theories.

6 Impact on Ionosphere and Thermosphere

Discrete auroral arcs enhance the E-region plasma density and increase ionospheric conductance within the arc by virtue of precipitating electrons accelerated within the auroral acceleration zone. Arcs that are not polarization arcs (Paschmann et al. 2003) (Chap. 6) are sustained by parallel currents that generate electric fields within the downward current region causing ionospheric heating via ion-neutral collisions. The heating may result in density cavities due to evacuation of current carriers and ion outflow. The enhanced electric fields and plasma density alter the E and F region neutral wind velocities through ion drag.

Discrete arcs contribute to about 16% of the total quiet time hemispherical precipitating energy flux (Newell et al. 2009). Electron density enhancements caused by precipitation within an arc can be greater than 2–3 times the background with typical densities ranging between 10^{11}–10^{12} m^{-3} peaking at about 105–120 km (Marklund et al. 1994; Kirkwood et al. 1988). Broadly speaking, the energy spectra associated with discrete arcs can be categorized into monoenergetic precipitation caused by electrostatic potential structures or broadband precipitation produced by Alfvénic acceleration. The peak energy of precipitating electrons within a discrete arc is around 1–10 keV, with electron energies increasing towards the center of the arc (Marklund et al. 1982). The precipitating energy flux is $\sim$1 mW/m^2 and can reach up to $\sim$15 mW/m^2 for Alfvénic acceleration (Colpitts et al. 2013). Precipitating electrons of energies up to 100 keV have also been observed on field lines conjugate with discrete auroral arcs (Swift and Gorney 1989). Higher mean electron energies can lead to a descent in the altitudes of maximum ionization and conductivity within the upward current region. An increase in the precipitating energy flux can lead to an increase in the maximum ionization and conductivity observed in this region. A statistical study by Deehr et al. (2005) has shown that the mean energy of precipitating electrons is higher in the day side of the dawn-dusk boundary, suggesting that a higher initial conductance (due to dayside photoionization) leads to greater acceleration. On the contrary, discrete arcs are frequently observed in the dusk to midnight sector. The reason may be that this region has low enough background ionospheric conductance and ion temperature for the ionospheric feedback instability (IFI) to develop and sustain them (Newell et al. 1996b, 2001).

Discrete arcs that are bounded by upward and downward field-aligned currents can be closed by a perpendicular Pedersen current in the horizontal plane. Observations from the CLUSTER satellites suggests the downward current region is dominated by current filaments of 10–20 km scale size in the ionosphere, with field-aligned current densities of a few $\mu A/m^2$ consistent with other studies (Wright et al. 2008). As mentioned in Sect. 3.5, the downward current region develops a depletion region, since the Pedersen current carries ions away and electrons flow upwards along the field line. The decreased plasma density results in a lower conductance that forces an increased electric field to sustain the same Pedersen current. The upward current region lies within the arc, and is 1–4 times narrower than the downward current-region. (Note that for the black aurora, satellite measurements show narrow downward current regions (Elphic et al. 1998; Marklund et al. 2001).) Due to electron precipitation the region has higher conductance, with field-aligned current densities reaching tens of $\mu A/m^2$ (Aikio et al. 2002). Smaller arc scale sizes may have higher field-aligned current densities (Juusola et al. 2016b; Stasiewicz and Potemra 1998).

Median Hall and Pedersen conductance ranges from 1–8 S and 1–6 S across MLT respectively, with minima located at dawn and maximum at $\sim$1–2 MLT (Aikio and Selkälä 2009). Within a stable discrete arc, the Hall and Pedersen conductance is higher than the background and can vary from $\sim$20–60 S and $\sim$8–29 S respectively (Kirkwood et al. 1988; Aikio et al. 2002). The magnitude of Hall and Pedersen currents carried within these arcs can

reach up to ∼1000 mA/m and ∼500 mA/m respectively (Aikio et al. 2002). In the dayside, since the background conductance is already high due to photoionization, arc formation is less favored and the conductance within the arc is only weakly increased from 0.5–1 S to 2–3 S (Nilsson et al. 2005). Discrete aurora mapped to the plasma-sheet boundary layer have high conductivities (Kirkwood et al. 1988), and their energy spectra fit the kappa distribution observed within the high-latitude plasma sheet (Kaeppler et al. 2014). The E-region electric fields within the discrete arcs are close to zero, while much stronger ($\gtrsim$50 mV/m) adjacent to them (Kirkwood et al. 1988).

The electric field enhancement excites the two stream instability leading to meter-scale electron density irregularities that backscatter radio waves called a Radar aurora (Bahcivan et al. 2006). Through ion-neutral collisions the enhanced electric field leads to frictional Joule heating. Median Joule heating rates are low during magnetically quiet times: 0–2 mW/m^2 with minimum in the dayside and maximum near 2 MLT (Aikio and Selkälä 2009). However, energy dissipation by both kinetic energy of particles and Joule heating can reach ∼100 mW/m^2 each (Marklund et al. 1982). The heating can cause the conversion of F region O^+ into NO^+ and result in faster recombination loss, since molecular ions have shorter chemical lifetimes. This results in additional loss of plasma density in the downward current region apart from upwelling or transport of current carriers out of the region (Zettergren and Semeter 2012). Since ion mobility is inversely proportional to collision frequency, and collision frequency increases with temperature, Joule heating causes the ion mobility to decrease. According to simulations by Streltsov (2008) this can suppress the IFI effectively. The result points to an additional reason for discrete arcs to be prevalent during night-time and the winter seasons: arcs attributed to IFI develop when ions in the ionosphere are cold.

Plasma flows of ∼340 to 720 m/s directed eastward were observed for two auroral arc filaments corresponding to southward electric fields of 18 and 40 mV/m using optical observations of afterglow of O^+ emissions (Dahlgren et al. 2009). Such flows can affect thermospheric wind velocities through enhanced ion drag due to the increased plasma density and localized ionospheric electric field associated with the auroral arc. In the E-region, the background neutral wind can rotate from the background wind field to align itself parallel along the discrete arc and revert back to the background flow direction when the arc disappears. In the particular case observed by Kosch et al. (2010), the wind rotations occurred within 7–16 minutes. In the F-region the effect is much weaker, but Zou et al. (2018) observed that the winds still exhibit a temporal evolution similar to the plasma flows but with a delay of $\lesssim$20 minutes, which is much faster than what was previously thought (a few hours). The neutral wind and plasma flow velocities are likely balanced by inertia and ion-drag with F-region neutral wind gaining about 19% of the plasma flow velocity gain (∼950 m/s) adjacent to the quasi-steady discrete arc studied in the above work. Arrays of Fabry-Perot interferometers can provide maps of neutral wind behavior for assimilation with radars and visible auroral imagery (Conde et al. 2001; Nicolls et al. 2012).

7 Generator and Magnetospheric Impact

The auroral arc (and aurora in general) is the low altitude effect of a complex magnetosphere/ionosphere/thermosphere coupling chain, sometimes called the auroral current circuit. The first suggestion on how this circuit looks came from Boström (1964), who identified two possible configurations, Type 1 and Type 2, presented in Fig. 15. Both Type 1 and Type 2 are discussed in more detail by Lysak et al. (this issue). Here we just note that, apart from the different topologies, in both cases electromagnetic energy is supplied by a

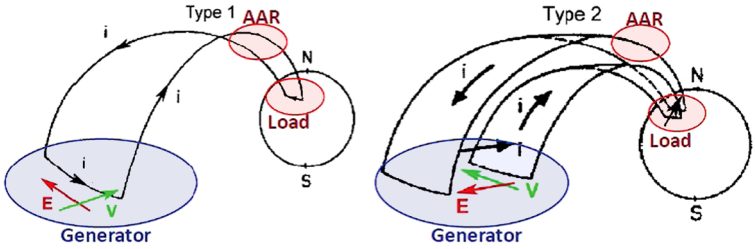

Fig. 15 The two basic configurations of the auroral current circuit suggested by Boström (1964): Type 1 (left) and Type 2 (right). Generator and load regions are indicated by blue and red shading, respectively. See text for more details. Adapted from Boström (1964)

magnetospheric generator region, where $\mathbf{E} \cdot \mathbf{i} < 0$, with $\mathbf{E}$ the electric field and $\mathbf{i}$ the current density. The mechanical energy of the plasma motion ($\mathbf{V}$ in Fig. 15) is converted into Poynting flux, transmitted along the auroral field lines to the ionospheric load, $\mathbf{E} \cdot \mathbf{i} > 0$, where it is converted back to mechanical energy by Joule heating.

After the original suggestion of Boström (1964), the understanding of the auroral current circuit was progressively consolidated and refined. A key milestone was the discovery and first systematic investigation of the AAR (indicated in Fig. 15), based on data from the S3-3 satellite (e.g. Mozer et al. 1980; Chiu et al. 1983). The acceleration of precipitating electrons and of outflowing ion beams (see more on ion beams below) occurs as well at the expense of the Poynting flux. Investigations based on Polar data indicated that the downward Poynting flux above the AAR is strong enough to feed auroral dissipation (e.g. Wygant et al. 2000), while statistical studies based on Polar (Keiling et al. 2002) and FAST (Chaston et al. 2002) data showed that energy flux is indeed dominated by Poynting flux above the AAR and by electron energy flux below the AAR (see the comparison by Chaston (2006), Fig. 16).

Among the three key regions of the auroral current circuit, the auroral ionosphere and the auroral acceleration region were explored far more intensively by satellite missions than the magnetospheric generator. Even though theoretical models and numerical simulations of auroral generator regions are well represented in the topical literature (see further details in Lysak et al., this issue) and Rostoker and Boström (1976), Lysak (1985), Vogt et al. (1999a), Birn and Hesse (2005), experimental evidence is scarce. Unlike the electrical circuits of daily life, where the various elements, including the generator, are localized (lumped), the key elements of the auroral current circuit are distributed over vast regions of space. While the power fed to the circuit is the integral over the generator volume and typically in the GW range, a satellite mission can only sample the local power density, $\mathbf{E} \cdot \mathbf{i}$, which can well be within the error margin. Moreover, one-spacecraft missions cannot infer the full current density vector, $\mathbf{i}$. With the launch of the four satellite Cluster mission (Escoubet et al. 2001), it became possible both to fully derive $\mathbf{i}$ and to improve the accuracy of the electric field estimates, due to the redundancy of the available data, such that a systematic search for generator regions became possible. The first results of an investigation along this line were published in two companion papers by Marghitu et al. (2006) and Hamrin et al. (2006), where conjugacy with low altitude inverted-V events observed by FAST provided further evidence on the connection of the observed generator regions to the aurora (Fig. 17).

Later on, this investigation was extended to a comprehensive survey of energy conversion regions (ECRs) in the plasma sheet, including concentrated generator regions (CGRs, $\mathbf{E} \cdot \mathbf{i} < 0$) and concentrated load regions (CLRs, $\mathbf{E} \cdot \mathbf{i} > 0$), where the term 'concentrated' indicates a local power density above the error margin of $\sim$1 pW/m^3. An outstanding result of

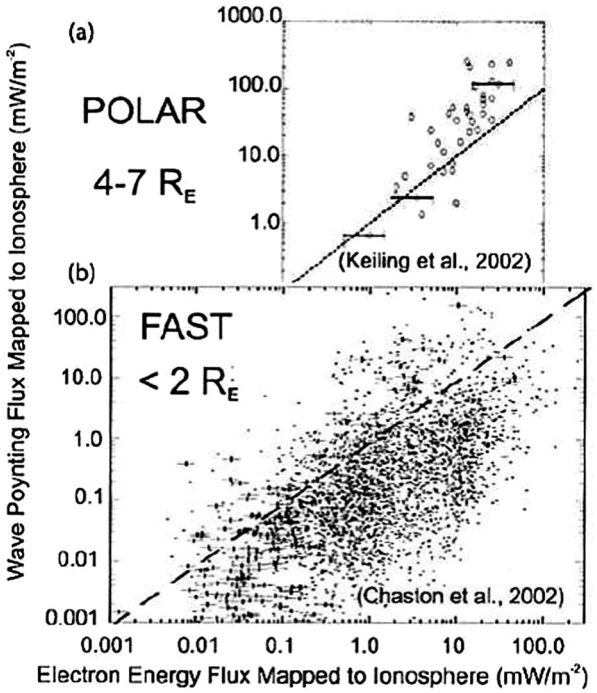

Fig. 16 Comparison of the Poynting flux and electron energy flux, as observed by the Polar satellite above the AAR (Keiling et al. 2002) and by the FAST satellite below the AAR (Chaston et al. 2002). After Chaston (2006)

this survey, summarized in the review by Hamrin et al. (2011), was that the observed ECRs were typically associated with bursty bulk flows (BBFs, Angelopoulos et al. 1992, 1994). Most of the ECRs were CLRs (as expected, considering the large scale load character of the plasma sheet), but the fraction of CGRs, of about one fifth, was significant too. In view of their statistical association with BBFs, it is likely that many of the observed CGRs actually fed their power to auroral streamers (not to auroral arcs). A closer examination of the energy conversion matter as related to the BBF structure and age was performed subsequently by Hamrin et al. (2013, 2014). Further details on BBFs and on their coupling to ionospheric streamers can be found in (Forsyth et al., this issue), as well as, e.g., in a recent review by Liu et al. (2018a).

The MI coupling chain described so far emphasizes the active role of the magnetosphere, that drives the auroral current circuit via generator regions, and suggests a rather passive role of the ionosphere, where energy is merely dissipated. However, energy dissipation generates in turn processes that feed back onto the magnetosphere and have an impact on the overall evolution of the MI system. An outstanding example of this feedback is the ion outflow, whose origin is in the ionospheric heating by Joule effect and electron precipitation. The gravitational binding of the heated ions is thus weakened and further heating processes, at higher altitudes, end up by ionospheric ion outflow injected into magnetosphere (e.g. Strangeway et al. 2005). The impact of the ionospheric ion outflow on the magnetosphere dynamics is diverse, ranging from the influence on the reconnection rate, through the speed of magnetospheric convection, to the rise and fall of the ring current (see e.g. Moore et al. 2014; Kronberg et al. 2014).

The ionospheric dissipation serves as well to relax the magnetic shear stress of the twisted flux tubes, again feeding back on the magnetospheric end, where the twisting proceeds. During active events the twisting prevails (note similarity with Boström Type 1), as reflected by

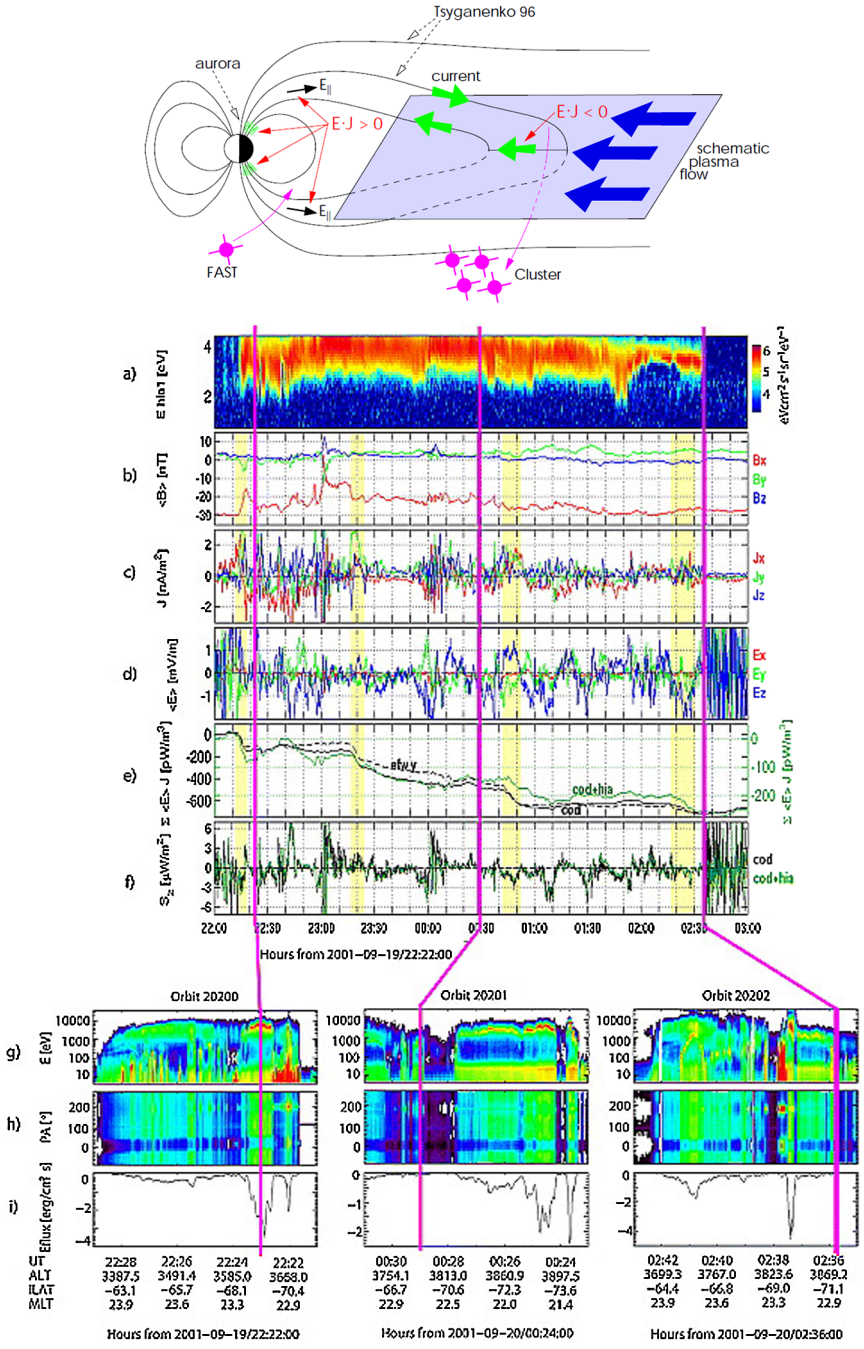

Fig. 17 Top: Schematic representation of the auroral current circuit, with the magnetospheric generator region sampled by the Cluster spacecraft and the low altitude end observed by the FAST satellite. From Hamrin et al. (2006). Bottom: Generator regions observed by Cluster in the magnetospheric plasma sheet (yellow stripes) conjugate (magenta lines) to inverted-V events observed by FAST at some 3000 km altitude above the auroral ionosphere. From the review by Hamrin et al. (2011), adapted after Marghitu et al. (2006) and Hamrin et al. (2006)

the large scale filamentary FAC of the substorm current wedge (McPherron et al. 1973; Keiling et al. 2009), or by meso-scale filamentary FACs associated with BBF-streamer current wedgelets (Birn et al., 2004; Liu et al., 2018). De-twisting dominates, e.g., during the (late) recovery stage of auroral substorms, when omega bands, threaded by meso-scale filamentary FACs, relax back to quiet arcs, threaded by (possibly undulated) sheet-like FACs (note, this time, similarity with Boström Type 2). A recent event study by Bunescu et al. (2017), based on Cluster observations conjugate to ground and FAST data, captured the progress of this process and suggested a relaxation time scale of about 10 min. The relevance of this time scale for the related magnetospheric processes and the specific auroral current circuit is yet to be explored.

The interhemispheric (a)symmetry of aurora provides another example where observations of low altitude features help understanding and, subsequently, diagnosing the coupled MI system, as well as the forcing exerted by the solar wind. Even though, at first sight, one may expect that auroras in the northern and southern hemispheres are merely symmetric images of each other, in reality this is not the case (e.g. Laundal and Østgaard 2009). As a matter of fact, as shown by both ground (e.g. Sato et al. 1998) and spacecraft (e.g. Østgaard et al. 2005) observations, asymmetry is rather the rule than the exception. As noted by Sato et al. (2015), perfect symmetry of conjugate auroras would require symmetric conditions both in the solar wind forcing and in the MI coupling chain. Considering the large number of potential asymmetries between the two hemispheres, many of which are essentially related to the asymmetric configuration of the magnetic field (Laundal et al. 2017), 'highly similar conjugate auroral events (...) are likely to be exceptionally rare in nature' (Sato et al. 2015). Specific drivers of interhemispheric asymmetries between conjugate auroras include the IMF components Bx and By, the difference in ionospheric conductance, and the difference in auroral acceleration, detailed, e.g., in the reviews by Østgaard et al. (2015) and Sato et al. (2015).

While the ionospheric footprint of the auroral region forms only one part of this complex magnetospheric/ionospheric/thermospheric coupling chain, its behaviour contains much information about the entire system. The visible signatures provide a movie of ongoing events; the electrodynamic signatures—**E** and **B**—connect the players, and the ionosphere and thermosphere, as revealed by radars, in situ observations, and neutral wind mappers, tell us the state of the footpoint. If we understand the physics of the auroral system, we can learn to read these signatures to constrain what can be happening in the far-dispersed magnetospheric regions.

8 Measurements Needed to Progress

Much of our understanding of auroral processes comes through a view of the auroral arc as an idealized sheetlike structure. This is an excellent startpoint that has provided a rich baseline for studying auroral plasma processes, particularly the details of both auroral acceleration processes, and of the effects of precipitation on the ionosphere and thermosphere. Many questions remain, however, as we move into system studies of the non-ideal aurora. Even sheetlike aurora have unaddressed physics in the longitudinal direction. And there is far more to the auroral system than sheetlike quiet arcs. We need to develop a firm understanding of the three-dimensional structure and time evolution of quiet arcs before we can tackle more complex morphologies such as westward surges and the interplay between discrete arcs and Alfvénic systems.

Moving beyond one-dimensional cuts of sheetlike arcs, what questions do we encounter? How does plasma flow into an arc region perpendicular to the magnetic field and perpendicular to the length of the arc? What magnetospheric generators create the need for auroral current systems? We can explore the ionospheric footprint of auroral current closure within a localized region, but examining the magnetospheric end will require development of closed theories of auroral physics. What allows an arc to remain relatively stable for many tens of minutes, and then abruptly change morphologies? What controls these shifts: magnetospheric drivers or ionospheric responses? What controls the plasma density profile both along and across the field line in the auroral zone? What are the rules of plasma transport at play here?

Various tools will help us move forward toward a more complete auroral theory. Modelling tools such as GITM and GEMINI allow us to decompose the three-dimensional volumetric region near an auroral arc into its various parameters and responses. These tools allow us to move beyond height-integrated idealized sheetlike systems into more complex morphologies. What happens to current closure as a sheetlike arc begins to bend? We can explore the responses we understand, in this complex environment, using volumetric models at a variety of resolutions. The new observations which are presently being planned also will move us in this direction. A variety of them involve the non-sheetlike system of the auroral zone, studied in a variety of multipoint and multidata fashions. The EISCAT3D will provide volumetric imaging (McCrea et al. 2015), and the continuation of the THEMIS GBO into multispectral information will be the means of extracting far more quantitative information from auroral imagery than simple whitelight images can provide. Other groundbased arrays and networks are designed to study not auroral physics at one point, but over a large field of view at high resolution. Finally, localized swarms of in situ high-resolution observations, following on and growing from the success of the recent ESA Swarm mission, and increasingly done in conjugacy with groundbased arrays, will fundamentally change our view from the idealized sheet to the real auroral arc.

Acknowledgements The authors are grateful for the kind hospitality of the International Space Science Institute (ISSI), Bern, Switzerland.

References

A.T. Aikio, A. Selkälä, Statistical properties of Joule heating rate, electric field and conductances at high latitudes. Ann. Geophys. **27**(7), 2661–2673 (2009). https://doi.org/10.5194/angeo-27-2661-2009. https://www.ann-geophys.net/27/2661/2009/

A.T. Aikio, T. Lakkala, A. Kozlovsky, P.J.S. Williams, Electric fields and currents of stable drifting auroral arcs in the evening sector. J. Geophys. Res. Space Phys. **107**(A12), 3–1314 (2002). https://doi.org/10.1029/2001JA009172. https://agupubs.onlinelibrary.wiley.com/doi/abs/10.1029/2001JA009172

A.T. Aikio, K. Mursula, S. Buchert, F. Forme, O. Amm, G. Marklund, M. Dunlop, D. Fontaine, A. Vaivads, A. Fazakerley, Temporal evolution of two auroral arcs as measured by the cluster satellite and coordinated ground-based instruments. Ann. Geophys. **22**(12), 4089–4101 (2004). https://doi.org/10.5194/angeo-22-4089-2004. https://www.ann-geophys.net/22/4089/2004/

A. Aikio, K. Mursula, S. Buchert, F. Forme, O. Amm, G. Marklund, M. Dunlop, D. Fontaine, A. Vaivads, A. Fazakerley, Temporal evolution of two auroral arcs as measured by the Cluster satellite and coordinated ground-based instruments, in *Annales Geophysicae*, vol. 22 (2004), pp. 4089–4101

A.T. Aikio, H. Vanhamäki, A.B. Workayehu, I.I. Virtanen, K. Kauristie, L. Juusola, S. Buchert, D. Knudsen, Swarm satellite and EISCAT radar observations of a plasma flow channel in the auroral oval near magnetic midnight. J. Geophys. Res. Space Phys. **123**(6), 5140–5158 (2018). https://doi.org/10.1029/2018JA025409. https://agupubs.onlinelibrary.wiley.com/doi/abs/10.1029/2018JA025409

S.-I. Akasofu, Dynamic morphology of auroras. Space Sci. Rev. **4**(4), 498–540 (1965)

S.-I. Akasofu, S. Chapman, A neutral line discharge theory of the aurora polaris. Philos. Trans. R. Soc. Lond. Ser. A, Math. Phys. Sci. **253**(1031), 359–406 (1961). https://doi.org/10.1098/rsta.1961.0004

S.-I. Akasofu, D. Kimball, C.-I. Meng, Dynamics of the aurora–VII equatorward motions and the multiplicity of auroral arcs. J. Atmos. Terr. Phys. **28**, 627–635 (1966)

S.-I. Akasofu, S. Chapman, P. Kendall, *The Significance of the Multiple Structure of the Auroral Arc* (1967)

L. Alm, G.T. Marklund, T. Karlsson, A. Masson, Pseudo altitude: a new perspective on the auroral density cavity. J. Geophys. Res. Space Phys. **118**(7), 4341–4351 (2013)

L. Alm, B. Li, G. Marklund, T. Karlsson, Statistical altitude distribution of the auroral density cavity. J. Geophys. Res. Space Phys. **120**(2), 996–1006 (2015)

L. Alm, G.T. Marklund, T. Karlsson, Electron density and parallel electric field distribution of the auroral density cavity. J. Geophys. Res. Space Phys. **120**(11), 9428–9441 (2015). https://doi.org/10.1002/2015JA021593. https://agupubs.onlinelibrary.wiley.com/doi/abs/10.1002/2015JA021593

O. Amm, A. Aruliah, S.C. Buchert, R. Fujii, J. Gjerloev, A. Ieda, T. Matsuo, C. Stolle, H. Vanhamäki, A. Yoshikawa, Towards understanding the electrodynamics of the 3-dimensional high-latitude ionosphere: present and future, in *Annales Geophysicae: Atmospheres, Hydrospheres and Space Sciences*, vol. 26 (2008), p. 3913

O. Amm, R. Fujii, K. Kauristie, A. Aikio, A. Yoshikawa, A. Ieda, H. Vanhamäki, A statistical investigation of the Cowling channel efficiency in the auroral zone. J. Geophys. Res. Space Phys. **116**(A2), A02304 (2011)

L. Andersson, R. Ergun, Acceleration of antiearthward electron fluxes in the auroral region. J. Geophys. Res. Space Phys. **111**(A7), A07203 (2006)

L. Andersson, R. Ergun, The search for double layers in space plasmas, in *Auroral Phenomenology and Magnetospheric Processes: Earth and Other Planets*. Geophys. Monogr. Ser., vol. 197 (2012)

L. Andersson, R. Ergun, D. Newman, J. McFadden, C. Carlson, Y.-J. Su, Characteristics of parallel electric fields in the downward current region of the aurora. Phys. Plasmas **9**(8), 3600–3609 (2002)

L. Andersson, D. Newman, R. Ergun, M. Goldman, C. Carlson, J. McFadden, Influence of suprathermal background electrons on strong auroral double layers: observations. Phys. Plasmas **15**(7), 072901 (2008)

V. Angelopoulos, W. Baumjohann, C. Kennel, F. Coroniti, M. Kivelson, R. Pellat, R. Walker, H. Lühr, G. Paschmann, Bursty bulk flows in the inner central plasma sheet. J. Geophys. Res. Space Phys. **97**(A4), 4027–4039 (1992)

V. Angelopoulos, C. Kennel, F. Coroniti, R. Pellat, M. Kivelson, R. Walker, C. Russell, W. Baumjohann, W. Feldman, J. Gosling, Statistical characteristics of bursty bulk flow events. J. Geophys. Res. Space Phys. **99**(11), 257–280 (1994). Paper 94ja01263

W. Archer, D.J. Knudsen, Distinguishing subauroral ion drifts from Birkeland current boundary flows. J. Geophys. Res. Space Phys. **123**, 819–826 (2018). https://doi.org/10.1002/2017JA024577

J. Archer, H. Dahlgren, N. Ivchenko, B. Lanchester, G. Marklund, Dynamics and characteristics of black aurora as observed by high-resolution ground-based imagers and radar. Int. J. Remote Sens. **32**(11), 2973–2985 (2011)

W.E. Archer, D.J. Knudsen, J.K. Burchill, B. Jackel, E. Donovan, M. Connors, L. Juusola, Birkeland current boundary flows. J. Geophys. Res. Space Phys. **122**(4), 4617–4627 (2017)

J.C. Armstrong, S.-I. Akasofu, G. Rostoker, A comparison of satellite observations of Birkeland currents with ground observations of visible aurora and ionospheric currents. J. Geophys. Res. **80**(4), 575–586 (1975)

G. Atkinson, Auroral arcs: result of the interaction of a dynamic magnetosphere with the ionosphere. J. Geophys. Res. **75**(25), 4746–4755 (1970). https://doi.org/10.1029/JA075i025p04746. https://agupubs.onlinelibrary.wiley.com/doi/abs/10.1029/JA075i025p04746

H. Bahcivan, D.L. Hysell, D. Lummerzheim, M.F. Larsen, R.F. Pfaff, Observations of colocated optical and radar aurora. J. Geophys. Res. **111**(A12), 12308 (2006). https://doi.org/10.1029/2006JA011923. http://doi.wiley.com/10.1029/2006JA011923

C.A. Barth, D.N. Baker, S.M. Bailey, Seasonal variation of auroral electron precipitation. Geophys. Res. Lett. **31**(4), L04809 (2004). https://doi.org/10.1029/2003GL018892. https://agupubs.onlinelibrary.wiley.com/doi/abs/10.1029/2003GL018892

J. Birn, M. Hesse, Energy release and conversion by reconnection in the magnetotail, in *Annales Geophysicae*, vol. 23 (2005), pp. 3365–3373

G.T. Blanchard, L.R. Lyons, J.C. Samson, F.J. Rich, Locating the polar cap boundary from observations of 6300 Å auroral emission. J. Geophys. Res. Space Phys. **100**(A5), 7855–7862 (1995). https://doi.org/10.1029/94JA02631. https://agupubs.onlinelibrary.wiley.com/doi/abs/10.1029/94JA02631

G.T. Blanchard, L.R. Lyons, J.C. Samson, Accuracy of using 6300 Å auroral emission to identify the magnetic separatrix on the nightside of Earth. J. Geophys. Res. Space Phys. **102**(A5), 9697–9703 (1997). https://doi.org/10.1029/96JA04000. https://agupubs.onlinelibrary.wiley.com/doi/abs/10.1029/96JA04000

E. Blixt, M. Kosch, J. Semeter, Relative drift between black aurora and the ionospheric plasma, in *Annales Geophysicae*, vol. 23 (2005), pp. 1611–1621

L.P. Block, C.-G. Fälthammar, P.-A. Lindqvist, G. Marklund, F. Mozer, A. Pedersen, T. Potemra, L. Zanetti, Electric field measurements on viking: first results. Geophys. Res. Lett. **14**(4), 435–438 (1987)

J.E. Borovsky, Auroral arc thicknesses as predicted by various theories. J. Geophys. Res. Space Phys. **98**(A4), 6101–6138 (1993)

R. Boström, A model of the auroral electrojets. J. Geophys. Res. **69**(23), 4983–4999 (1964)

A. Boudouridis, H.E. Spence, Separation of spatial and temporal structure of auroral particle precipitation. J. Geophys. Res. Space Phys. **112**(A12), A12217 (2007)

W. Bristow, G. Sofko, H. Stenbaek-Nielsen, S. Wei, D. Lummerzheim, A. Otto, Detailed analysis of substorm observations using superDARN, UVI, ground-based magnetometers, and all-sky imagers. J. Geophys. Res. Space Phys. **108**(A3), 1124 (2003). https://doi.org/10.1029/2002JA009242

P. Carlqvist, R. Boström, Space-charge regions above the aurora. J. Geophys. Res. **75**(34), 7140–7146 (1970)

C. Carlson, R. Pfaff, J. Watzin, The FAST Auroral SnapshoT (FAST) mission. Geophys. Res. Lett. **25**(12), 2013–2016 (1998a)

C. Carlson, J. McFadden, R. Ergun, M. Temerin, W. Peria, F. Mozer, D. Klumpar, E. Shelley, W. Peterson, E. Moebius, et al., Fast observations in the downward auroral current region: energetic upgoing electron beams, parallel potential drops, and ion heating. Geophys. Res. Lett. **25**(12), 2017–2020 (1998b)

C. Cattell, L. Johnson, R. Bergmann, D. Klumpar, C. Carlson, J. McFadden, R. Strangeway, R. Ergun, K. Sigsbee, R. Pfaff, FAST observations of discrete electrostatic waves in association with down-going ion beams in the auroral zone. J. Geophys. Res. Space Phys. **107**(A9), 1238 (2002)

C. Cattell, J. Dombeck, L. Hanson, Solar cycle effects on parallel electric field acceleration of auroral electron beams. J. Geophys. Res. Space Phys. **118**(9), 5673–5680 (2013). https://doi.org/10.1002/jgra.50546. https://agupubs.onlinelibrary.wiley.com/doi/abs/10.1002/jgra.50546

S. Chapman, The electrical conductivity of the ionosphere: a review. Nuovo Cimento (1955–1965) **4**, 1385–1412 (1956)

C. Chaston, ULF waves and auroral electrons, in *Magnetospheric ULF Waves: Synthesis and New Directions*, vol. 169 (2006), pp. 239–257

C.C. Chaston, Magnetic reconnection in the auroral acceleration region. Geophys. Res. Lett. **42**(6), 1646–1653 (2015). https://doi.org/10.1002/2015GL063164. https://agupubs.onlinelibrary.wiley.com/doi/abs/10.1002/2015GL063164

C. Chaston, J. Bonnell, C. Carlson, M. Berthomier, L. Peticolas, I. Roth, J. McFadden, R. Ergun, R. Strangeway, Electron acceleration in the ionospheric Alfven resonator. J. Geophys. Res. Space Phys. **107**(A11), 41 (2002)

Y. Chiu, J. Cornwall, J. Fennell, D. Gorney, P. Mizera, Auroral plasmas in the evening sector: satellite observations and theoretical interpretations. Space Sci. Rev. **35**(3), 211–257 (1983)

A. Christensen, L. Lyons, J. Hecht, G. Sivjee, R. Meier, D. Strickland, Magnetic field-aligned electric field acceleration and the characteristics of the optical aurora. J. Geophys. Res. Space Phys. **92**(A6), 6163–6167 (1987)

R. Clayton, M. Burleigh, K. Lynch, M. Zettergren, M. Conde, T. Evans, G. Grubbs, D. Hampton, D. Hysell, M. Lessard, R. Michell, A. Reimer, T.M. Roberts, M. Samara, R. Varney, 3d modeling results of the GEMINI model using reconstructed 2d maps of auroral data (2019a), in preparation

R. Clayton, K. Lynch, M. Zettergren, M. Burleigh, M. Conde, G. Grubbs, D. Hampton, D. Hysell, M. Lessard, R. Michell, A. Reimer, T.M. Roberts, M. Samara, R. Varney, Two-dimensional maps of in situ ionospheric plasma flow data near auroral arcs using auroral imagery. J. Geophys. Res. Space Phys. **124**(4), 3036–3056 (2019b). https://doi.org/10.1029/2018JA026440. https://agupubs.onlinelibrary.wiley.com/doi/abs/10.1029/2018JA026440

C.A. Colpitts, S. Hakimi, C.A. Cattell, J. Dombeck, M. Maas, Simultaneous ground and satellite observations of discrete auroral arcs, substorm aurora, and Alfvénic aurora with FAST and THEMIS GBO. J. Geophys. Res. Space Phys. **118**(11), 6998–7010 (2013). https://doi.org/10.1002/2013JA018796. http://doi.wiley.com/10.1002/2013JA018796

M. Conde, J.D. Craven, T. Immel, E. Hoch, H. Stenbaek-Nielsen, T. Hallinan, R.W. Smith, J. Olson, W. Sun, L.A. Frank, J. Sigwarth, Assimilated observations of thermospheric winds, the aurora, and ionospheric currents over Alaska. J. Geophys. Res. Space Phys. **106**(A6), 10493–10508 (2001). https://doi.org/10.1029/2000JA000135. https://agupubs.onlinelibrary.wiley.com/doi/abs/10.1029/2000JA000135

B. Coppi, G. Laval, R. Pellat, Dynamics of the geomagnetic tail. Phys. Rev. Lett. **16**, 1207–1210 (1966). https://doi.org/10.1103/PhysRevLett.16.1207. https://link.aps.org/doi/10.1103/PhysRevLett.16.1207

T. Cowling, Magnetism, solar: the electrical conductivity of an ionised gas in the presence of a magnetic field. Mon. Not. R. Astron. Soc. **93**, 90 (1932)

H. Dahlgren, N. Ivchenko, B.S. Lanchester, M. Ashrafi, D. Whiter, G. Marklund, J. Sullivan, First direct optical observations of plasma flows using afterglow of O+ in discrete aurora. J. Atmos. Sol.-Terr. Phys. **71**(2), 228–238 (2009). https://doi.org/10.1016/J.JASTP.2008.11.015. https://www.sciencedirect.com/science/article/pii/S1364682608003751?via%3Dihub

T.N. Davis, Observed characteristics of auroral forms. Space Sci. Rev. **22**(1), 77–113 (1978). https://doi.org/10.1007/BF00215814.

C. Deehr, D. Lummerzheim, Ground-based optical observations of hydrogen emission in the auroral substorm. J. Geophys. Res. Space Phys. **106**(A1), 33–44 (2001). https://doi.org/10.1029/2000JA002010. https://agupubs.onlinelibrary.wiley.com/doi/abs/10.1029/2000JA002010

C.S. Deehr, M.H. Rees, A.E.H. Belon, G.J. Romick, D. Lummerzheim, Influence of the ionosphere on the altitude of discrete auroral arcs. Ann. Geophys. **23**(3), 759–766 (2005). https://doi.org/10.5194/angeo-23-759-2005. http://www.ann-geophys.net/23/759/2005/

R.A. Doe, M. Mendillo, J.F. Vickrey, L.J. Zanetti, R.W. Eastes, Observations of nightside auroral cavities. J. Geophys. Res. Space Phys. **98**(A1), 293–310 (1993)

R. Doe, M. Mendillo, J. Vickrey, J. Ruohoniemi, R. Greenwald, Coordinated convection measurements in the vicinity of auroral cavities. Radio Sci. **29**(1), 293–309 (1994)

E.F. Donovan, B.J. Jackel, I. Voronkov, T. Sotirelis, F. Creutzberg, N.A. Nicholson, Ground-based optical determination of the b2i boundary: a basis for an optical MT-index. J. Geophys. Res. Space Phys. **108**(A3), 1115 (2003). https://doi.org/10.1029/2001JA009198. https://agupubs.onlinelibrary.wiley.com/doi/abs/10.1029/2001JA009198

E. Donovan, W. Liu, J. Liang, E. Spanswick, I. Voronkov, M. Connors, M. Syrjäsuo, G. Baker, B. Jackel, T. Trondsen, M. Greffen, V. Angelopoulos, C.T. Russell, S.B. Mende, H.U. Frey, A. Keiling, C.W. Carlson, J.P. McFadden, K.-H. Glassmeier, U. Auster, K. Hayashi, K. Sakaguchi, K. Shiokawa, J.A. Wild, I.J. Rae, Simultaneous THEMIS in situ and auroral observations of a small substorm. Geophys. Res. Lett. **35**(17), L17S18 (2008). https://doi.org/10.1029/2008GL033794. https://agupubs.onlinelibrary.wiley.com/doi/abs/10.1029/2008GL033794

R. Elphic, J. Bonnell, R. Strangeway, L. Kepko, R. Ergun, J. McFadden, C. Carlson, W. Peria, C. Cattell, D. Klumpar, et al., The auroral current circuit and field-aligned currents observed by fast. Geophys. Res. Lett. **25**(12), 2033–2036 (1998)

R. Elphinstone, J. Murphree, L. Cogger, What is a global auroral substorm? Rev. Geophys. **34**(2), 169–232 (1996)

R. Ergun, L. Andersson, D. Main, Y.-J. Su, C. Carlson, J. McFadden, F. Mozer, Parallel electric fields in the upward current region of the aurora: indirect and direct observations. Phys. Plasmas **9**(9), 3685–3694 (2002a)

R. Ergun, L. Andersson, D. Main, Y.-J. Su, D. Newman, M. Goldman, C. Carlson, J. McFadden, F. Mozer, Parallel electric fields in the upward current region of the aurora: numerical solutions. Phys. Plasmas **9**(9), 3695–3704 (2002b)

R. Ergun, L. Andersson, C. Carlson, D. Newman, M. Goldman, Double layers in the downward current region of the aurora. Nonlinear Process. Geophys. **10**(1/2), 45–52 (2003)

R. Ergun, L. Andersson, D. Main, Y.-J. Su, D. Newman, M. Goldman, C. Carlson, A. Hull, J. McFadden, F. Mozer, Auroral particle acceleration by strong double layers: the upward current region. J. Geophys. Res. Space Phys. **109**(A12), A12220 (2004)

C. Escoubet, M. Fehringer, M. Goldstein, The cluster mission—introduction, in *Annales Geophysicae*, vol. 19, (Eur. Math. Soc., Lindau, 2001), pp. 1197–1200

D.S. Evans, The observations of a near monoenergetic flux of auroral electrons. J. Geophys. Res. **73**(7), 2315–2323 (1968)

D.S. Evans, Precipitating electron fluxes formed by a magnetic field aligned potential difference. J. Geophys. Res. **79**(19), 2853–2858 (1974)

D.S. Evans, The characteristics of a persistent auroral arc at high latitude in the 1400 MLT sector, in *The Polar Cusp*, ed. by J.A. Holtet, A. Egeland (Springer, Dordrecht, 1985), pp. 99–109. ISBN 978-94-009-5295-9

S. Figueiredo, G. Marklund, T. Karlsson, T. Johansson, Y. Ebihara, M. Ejiri, N. Ivchenko, P.-A. Lindqvist, H. Nilsson, A. Fazakerley, Temporal and spatial evolution of discrete auroral arcs as seen by cluster. Ann. Geophys. **23**(7), 2531–2557 (2005)

C. Forsyth, A. Fazakerley, A. Walsh, C.E. Watt, K. Garza, C. Owen, D. Constantinescu, I. Dandouras, K.-H. Fornaçon, E. Lucek, et al., Temporal evolution and electric potential structure of the auroral acceleration region from multispacecraft measurements. J. Geophys. Res. Space Phys. **117**(A12), A12203 (2012)

H.U. Frey, O. Amm, C.C. Chaston, S. Fu, G. Haerendel, L. Juusola, T. Karlsson, B. Lanchester, R. Nakamura, N. Østgaard, T. Sakanoi, E. Séran, D. Whiter, J. Weygand, K. Asamura, M. Hirahara, Small and

meso-scale properties of a substorm onset auroral arc. J. Geophys. Res. Space Phys. **115**(A10), A10209 (2010a). https://doi.org/10.1029/2010JA015537. https://agupubs.onlinelibrary.wiley.com/doi/abs/10.1029/2010JA015537

H. Frey, O. Amm, C. Chaston, S. Fu, G. Haerendel, L. Juusola, T. Karlsson, B. Lanchester, R. Nakamura, N. Østgaard, et al., Small and meso-scale properties of a substorm onset auroral arc. J. Geophys. Res. Space Phys. **115**(A10), A10209 (2010b). https://doi.org/10.1029/2010JA015537

E. Friis-Christensen, H. Lühr, D. Knudsen, R. Haagmans, Swarm–an Earth observation mission investigating geospace. Adv. Space Res. **41**(1), 210–216 (2008)

R. Fujii, O. Amm, A. Yoshikawa, A. Ieda, H. Vanhamäki, Reformulation and energy flow of the Cowling channel. J. Geophys. Res. Space Phys. **116**(A2), A02305 (2011)

R. Fujii, O. Amm, H. Vanhamäki, A. Yoshikawa, A. Ieda, An application of the finite length Cowling channel model to auroral arcs with longitudinal variations. J. Geophys. Res. Space Phys. **117**(A11), A11217 (2012)

Y.I. Galperin, Multiple scales in auroral plasmas. J. Atmos. Sol.-Terr. Phys. **64**(2), 211–229 (2002)

D.M. Gillies, D.J. Knudsen, E.F. Donovan, E.L. Spanswick, C. Hansen, D. Keating, S. Erion, A survey of quiet auroral arc orientation and the effects of the interplanetary magnetic field. J. Geophys. Res. Space Phys. **119**(4), 2550–2562 (2014). https://doi.org/10.1002/2013JA019469. https://agupubs.onlinelibrary.wiley.com/doi/abs/10.1002/2013JA019469

D. Gillies, D. Knudsen, E. Spanswick, E. Donovan, J. Burchill, M. Patrick, Swarm observations of field-aligned currents associated with pulsating auroral patches. J. Geophys. Res. Space Phys. **120**(11), 9484–9499 (2015). https://doi.org/10.1002/2015JA021416

D.M. Gillies, D. Knudsen, R. Rankin, S. Milan, E. Donovan, A statistical survey of the 630.0 nm optical signature of periodic auroral arcs resulting from magnetospheric field line resonances. Geophys. Res. Lett. **45**, 4648–4655 (2018)

J. Gjerloev, S. Ohtani, T. Iijima, B. Anderson, J. Slavin, G. Le, Characteristics of the terrestrial field-aligned current system. Ann. Geophys. **29**(10) 1713–1729 (2011)

G. Grubbs II, R. Michell, M. Samara, D. Hampton, J.-M. Jahn, Predicting electron population characteristics in 2-d using multispectral ground-based imaging. Geophys. Res. Lett. **45**(1), 15–20 (2018). https://doi.org/10.1002/2017GL075873. https://agupubs.onlinelibrary.wiley.com/doi/abs/10.1002/2017GL075873

G. Grubbs, R. Michell, M. Samara, D. Hampton, J. Hecht, S. Solomon, J.-M. Jahn, A comparative study of spectral auroral intensity predictions from multiple electron transport models. J. Geophys. Res. Space Phys. **123**(1), 993–1005 (2018a)

G. Grubbs, R. Michell, M. Samara, D. Hampton, J.-M. Jahn, Predicting electron population characteristics in 2-d using multispectral ground-based imaging. Geophys. Res. Lett. **45**(1), 15–20 (2018b)

D.A. Gurnett, Electric Field and Plasma Observations in the Magnetosphere, Technical report, Iowa Univ. Iowa City Dept. Of Physics and Astronomy, 1972

B. Gustavsson, M.J. Kosch, A. Senior, A.J. Kavanagh, B. Brändström, E. Blixt, Combined EISCAT radar and optical multispectral and tomographic observations of black aurora. J. Geophys. Res. Space Phys. **113**(A6), A06308 (2008)

G. Haerendel, Acceleration from field-aligned potential drops. Int. Astron. Union Colloq. **142**, 765–774 (1994). https://doi.org/10.1017/S0252921100078076

G. Haerendel, H. Frey, Role and origin of the poleward Alfvénic arc. J. Geophys. Res. Space Phys. **119**(4), 2945–2962 (2014). https://doi.org/10.1002/2014JA019786

G. Haerendel, H.U. Frey, C.C. Chaston, O. Amm, L. Juusola, R. Nakamura, E. Seran, J. Weygand, Birth and life of auroral arcs embedded in the evening auroral oval convection: a critical comparison of observations with theory. J. Geophys. Res. Space Phys. **117**(A12), A12220 (2012). https://doi.org/10.1029/2012JA018128

T.J. Hallinan, T.N. Davis, Small-scale auroral arc distortions. Planet. Space Sci. **18**(12), 1735–1744 (1970)

T. Hallinan, H. Stenbaek-Nielsen, The connection between auroral acceleration and auroral morphology. Phys. Chem. Earth, Part C, Sol.-Terr. Planet. Sci. **26**(1–3), 169–177 (2001)

T.J. Hallinan, J. Kimball, H.C. Stenbaek-Nielsen, K. Lynch, R. Arnoldy, J. Bonnell, P. Kintner, Relation between optical emissions, particles, electric fields, and Alfvén waves in a multiple rayed arc. J. Geophys. Res. **106**, 15445 (2001)

T.J. Hallinan, J. Kimball, H.C. Stenbaek-Nielsen, K. Lynch, R. Arnoldy, J. Bonnell, P. Kintner, Relation between optical emissions, particles, electric fields, and Alfvén waves in a multiple rayed arc. J. Geophys. Res. Space Phys. **106**(A8), 15445–15454 (2001). https://doi.org/10.1029/2000JA000321. https://agupubs.onlinelibrary.wiley.com/doi/abs/10.1029/2000JA000321

M. Hamrin, O. Marghitu, K. Rönnmark, B. Klecker, M. André, S. Buchert, L. Kistler, J. McFadden, H. Reme, A. Vaivads, Observations of concentrated generator regions in the nightside magnetosphere by Cluster/FAST conjunctions, in *Annales Geophysicae*, vol. 24 (2006), pp. 637–649

M. Hamrin, O. Marghitu, P. Norqvist, S. Buchert, M. André, B. Klecker, L.M. Kistler, I. Dandouras, Energy conversion regions as observed by cluster in the plasma sheet. J. Geophys. Res. Space Phys. **116**(A1), A00K08 (2011)

M. Hamrin, P. Norqvist, T. Karlsson, H. Nilsson, H. Fu, S. Buchert, M. André, O. Marghitu, T. Pitkänen, B. Klecker, et al., The evolution of flux pileup regions in the plasma sheet: cluster observations. J. Geophys. Res. Space Phys. **118**(10), 6279–6290 (2013)

M. Hamrin, T. Pitkänen, P. Norqvist, T. Karlsson, H. Nilsson, M. André, S. Buchert, A. Vaivads, O. Marghitu, B. Klecker, et al., Evidence for the braking of flow bursts as they propagate toward the Earth. J. Geophys. Res. Space Phys. **119**(11), 9004–9018 (2014)

P. Hanna, C. Anger, Auroral colour variations. Planet. Space Sci. **19**(4), 399–411 (1971)

Z.-J. Hu, H. Yang, D. Huang, T. Araki, N. Sato, M. Taguchi, E. Seran, H. Hu, R. Liu, B. Zhang, D. Han, Z. Chen, Q. Zhang, J. Liang, S. Liu, Synoptic distribution of dayside aurora: multiple-wavelength all-sky observation at yellow river station in ny-Ålesund, svalbard. J. Atmos. Sol.-Terr. Phys. **71**(8), 794–804 (2009). https://doi.org/10.1016/j.jastp.2009.02.010. http://www.sciencedirect.com/science/article/pii/S1364682609000339

A. Hull, J. Bonnell, F. Mozer, J. Scudder, C. Chaston, Large parallel electric fields in the upward current region of the aurora: evidence for ambipolar effects. J. Geophys. Res. Space Phys. **108**(A6), 1265 (2003a)

A. Hull, J. Bonnell, F. Mozer, J. Scudder, A statistical study of large-amplitude parallel electric fields in the upward current region of the auroral acceleration region. J. Geophys. Res. Space Phys. **108**(A1), 1007 (2003b)

A. Hull, C. Chaston, H. Frey, M. Fillingim, M. Goldstein, J. Bonnell, F. Mozer, The "Alfvénic surge" at substorm onset/expansion and the formation of "Inverted Vs": Cluster and IMAGE observations. J. Geophys. Res. Space Phys. **121**(5), 3978–4004 (2016)

B. Hultqvist, Downward ion acceleration at auroral latitudes: cause of parallel electric field, in *Annales Geophysicae*, vol. 20 (2002), pp. 1117–1136

K.-J. Hwang, K. Lynch, C. Carlson, J. Bonnell, W. Peria, Fast auroral snapshot observations of perpendicular dc electric field structures in downward auroral current regions: morphology. J. Geophys. Res. Space Phys. **111**(A9), A09205 (2006a)

K.-J. Hwang, K. Lynch, C. Carlson, J. Bonnell, W. Peria, Fast auroral snapshot observations of perpendicular DC electric field structures in downward current regions: implications. J. Geophys. Res. Space Phys. **111**(A9), A09206 (2006b)

K.-J. Hwang, R. Ergun, L. Andersson, D. Newman, C. Carlson, Test particle simulations of the effect of moving DLs on ion outflow in the auroral downward-current region. J. Geophys. Res. Space Phys. **113**(A1), A01308 (2008)

T. Iijima, T.A. Potemra, The amplitude distribution of field-aligned currents at northern high latitudes observed by triad. J. Geophys. Res. **81**(13), 2165–2174 (1976)

P. Israelevich, I. Podgorny, A. Kuzmin, N. Nikolaeva, E. Dubinin, Convection and field-aligned currents, related to polar cap arcs, during strongly northward IMF (11 January 1983). Planet. Space Sci. **36**(12), 1317–1328 (1988)

P.T. Jayachandran, E.F. Donovan, J.W. MacDougall, D.R. Moorcroft, J.-P. St. Maurice, P. Prikryl, Superdarn e-region backscatter boundary in the dusk-midnight sector—tracer of equatorward boundary of the auroral oval. Ann. Geophys. **20**(12), 1899–1904 (2002). https://doi.org/10.5194/angeo-20-1899-2002. https://www.ann-geophys.net/20/1899/2002/

F. Jiang, R.J. Strangeway, M.G. Kivelson, J.M. Weygand, R.J. Walker, K.K. Khurana, Y. Nishimura, V. Angelopoulos, E. Donovan, In situ observations of the "preexisting auroral arc" by themis all sky imagers and the fast spacecraft. J. Geophys. Res. Space Phys. **117**(A5) (2012). https://doi.org/10.1029/2011JA017128. https://agupubs.onlinelibrary.wiley.com/doi/abs/10.1029/2011JA017128

F. Jiang, M.G. Kivelson, R.J. Strangeway, K.K. Khurana, R. Walker, Ionospheric flow shear associated with the preexisting auroral arc: a statistical study from the fast spacecraft data. J. Geophys. Res. Space Phys. **120**(6), 5194–5213 (2015a). https://doi.org/10.1002/2013JA019255. https://agupubs.onlinelibrary.wiley.com/doi/abs/10.1002/2013JA019255

F. Jiang, M.G. Kivelson, R.J. Strangeway, K.K. Khurana, R. Walker, Ionospheric flow shear associated with the preexisting auroral arc: a statistical study from the FAST spacecraft data. J. Geophys. Res. Space Phys. **120**(6), 5194–5213 (2015b)

T. Johansson, G. Marklund, T. Karlsson, S. Liléo, P.-A. Lindqvist, A. Marchaudon, H. Nilsson, A. Fazakerley, On the profile of intense high-altitude auroral electric fields at magnetospheric boundaries, in *Annales Geophysicae*, vol. 24 (2006), pp. 1713–1723

T. Johansson, G. Marklund, T. Karlsson, S. Liléo, P.-A. Lindqvist, H. Nilsson, S. Buchert, Scale sizes of intense auroral electric fields observed by Cluster, in *Annales Geophysicae*, vol. 25 (2007), pp. 2413–2425

M.G. Johnsen, D.A. Lorentzen, A statistical analysis of the optical dayside open/closed field line boundary. J. Geophys. Res. Space Phys. **117**(A2), A02218 (2012). https://doi.org/10.1029/2011JA016984. https://agupubs.onlinelibrary.wiley.com/doi/abs/10.1029/2011JA016984

J.R.T. Jussila, A.T. Aikio, S. Shalimov, S.R. Marple, Cosmic radio noise absorption events associated with equatorward drifting arcs during a substorm growth phase. Ann. Geophys. **22**(5), 1675–1686 (2004). https://doi.org/10.5194/angeo-22-1675-2004. https://www.ann-geophys.net/22/1675/2004/

L. Juusola, K. Kauristie, H. Vanhamäki, A. Aikio, M. Kamp, Comparison of auroral ionospheric and field-aligned currents derived from swarm and ground magnetic field measurements. J. Geophys. Res. Space Phys. **121**(9), 9256–9283 (2016a)

L. Juusola, W.E. Archer, K. Kauristie, J.K. Burchill, H. Vanhamäki, A.T. Aikio, Ionospheric conductances and currents of a morning sector auroral arc from Swarm-A electric and magnetic field measurements. Geophys. Res. Lett. **43**(22), 11519–11527 (2016b). https://doi.org/10.1002/2016GL070248. http://doi.wiley.com/10.1002/2016GL070248

S.R. Kaeppler, M.J. Nicolls, A. Strømme, C.A. Kletzing, S.R. Bounds, Observations in the E region ionosphere of kappa distribution functions associated with precipitating auroral electrons and discrete aurorae. J. Geophys. Res. Space Phys. **119**(12), 10164–10183 (2014). https://doi.org/10.1002/2014JA020356. http://doi.wiley.com/10.1002/2014JA020356

Y. Kamide, S.-I. Akasofu, The location of the field-aligned currents with respect to discrete auroral arcs. J. Geophys. Res. **81**(22), 3999–4003 (1976)

T. Karlsson, The acceleration region of stable auroral arcs, in *Chapman Conference on the Relationship Between Auroral Phenomenology and Magnetospheric Processes*, Feb. 27–Mar. 04, 2011, Fairbanks, AK (Am. Geophys. Union, Washington, 2012), pp. 227–239

T. Karlsson, *The Acceleration Region of Stable Auroral Arcs* (Am. Geophys. Union, Washington, 2013), pp. 227–240. https://doi.org/10.1029/2011GM001179. https://agupubs.onlinelibrary.wiley.com/doi/abs/10.1029/2011GM001179

T. Karlsson, G. Marklund, A statistical study of intense low-altitude electric fields observed by freja. Geophys. Res. Lett. **23**(9), 1005–1008 (1996)

T. Karlsson, G. Marklund, N. Brenning, I. Axnäs, On enhanced aurora and low-altitude parallel electric fields. Phys. Scr. **72**(5), 419 (2005)

T. Karlsson, N. Brenning, O. Marghitu, G. Marklund, S. Buchert, High-altitude signatures of ionospheric density depletions caused by field-aligned currents. arXiv preprint, arXiv:0704.1610 (2007)

A. Keiling, J. Wygant, C. Cattell, W. Peria, G. Parks, M. Temerin, F. Mozer, C. Russell, C. Kletzing, Correlation of Alfvén wave poynting flux in the plasma sheet at 4–7 RE with ionospheric electron energy flux. J. Geophys. Res. Space Phys. **107**(A7), 24 (2002)

A. Keiling, V. Angelopoulos, A. Runov, J. Weygand, S. Apatenkov, S. Mende, J. McFadden, D. Larson, O. Amm, K.-H. Glassmeier, et al., Substorm current wedge driven by plasma flow vortices: themis observations. J. Geophys. Res. Space Phys. **114**(A1), A00C22 (2009)

J. Kimball, T. Hallinan, Observations of black auroral patches and of their relationship to other types of aurora. J. Geophys. Res. Space Phys. **103**(A7), 14671–14682 (1998)

P.M. Kintner, H. Kil, C. Deehr, P. Schuck, Simultaneous total electron content and all-sky camera measurements of an auroral arc. J. Geophys. Res. Space Phys. **107**(A7), 13–1136 (2002). https://doi.org/10.1029/2001JA000110. https://agupubs.onlinelibrary.wiley.com/doi/abs/10.1029/2001JA000110

S. Kirkwood, H. Opgenoorth, J.S. Murphree, Ionospheric conductivities, electric fields and currents associated with auroral substorms measured by the EISCAT radar. Planet. Space Sci. **36**(12), 1359–1380 (1988). https://doi.org/10.1016/0032-0633(88)90005-0. https://www.sciencedirect.com/science/article/pii/0032063388900050?via%3Dihub

D. Klumpar, W. Heikkila, Electrons in the ionospheric source cone: evidence for runaway electrons as carriers of downward Birkeland currents. Geophys. Res. Lett. **9**(8), 873–876 (1982)

S. Knight, Parallel electric fields. Planet. Space Sci. **21**(5), 741–750 (1973)

D.J. Knudsen, Spatial modulation of electron energy and density by nonlinear stationary inertial Alfvén waves. J. Geophys. Res. Space Phys. **101**(A5), 10761–10772 (1996). https://doi.org/10.1029/96JA00429

D. Knudsen, E. Donovan, L. Cogger, B. Jackel, W. Shaw, Width and structure of mesoscale optical auroral arcs. Geophys. Res. Lett. **28**(4), 705–708 (2001)

M.J. Kosch, C. Anderson, R.A. Makarevich, B.A. Carter, R.A.D. Fiori, M. Conde, P.L. Dyson, T. Davies, First *E* region observations of mesoscale neutral wind interaction with auroral arcs. J. Geophys. Res. Space Phys. **115**(A2) A02303, (2010). https://doi.org/10.1029/2009JA014697. http://doi.wiley.com/10.1029/2009JA014697

A. Kozlovsky, T. Lakkala, J. Kangas, A. Aikio, Response of the quiet auroral arc motion to ionospheric convection variations. J. Geophys. Res. Space Phys. **106**(A10), 21463–21473 (2001). https://doi.org/10.1029/2001JA900043. https://agupubs.onlinelibrary.wiley.com/doi/abs/10.1029/2001JA900043

A.E. Kozlovsky, V.V. Safargaleev, J.R.T. Jussila, A.V. Koustov, Pre-noon high-latitude auroral arcs as a manifestation of the interchange instability. Ann. Geophys. **21**(12), 2303–2314 (2003). https://doi.org/10.5194/angeo-21-2303-2003. https://www.ann-geophys.net/21/2303/2003/

A.E. Kozlovsky, H. Nilsson, V.V. Safargaleev, Complex study of the auroral arc dynamics and ionospheric plasma convection in prenoon hours. Geomagn. Aeron. **46**(4), 473–484 (2006). https://doi.org/10.1134/S0016793206040098.

A. Kozlovsky, T. Turunen, S. Massetti, Field-aligned currents of postnoon auroral arcs. J. Geophys. Res. Space Phys. **114**(A3), A03301 (2009)

E.A. Kronberg, M. Ashour-Abdalla, I. Dandouras, D.C. Delcourt, E.E. Grigorenko, L.M. Kistler, I.V. Kuzichev, J. Liao, R. Maggiolo, H.V. Malova, et al., Circulation of heavy ions and their dynamical effects in the magnetosphere: recent observations and models. Space Sci. Rev. **184**(1-4), 173–235 (2014)

B. Lanchester, B. Gustavsson, Imaging of aurora to estimate the energy and flux of electron precipitation, in *Auroral Phenomenology and Magnetospheric Processes: Earth and Other Planets*, vol. 197 (2012), pp. 171–182

K. Laundal, N. Østgaard, Asymmetric auroral intensities in the Earth's northern and southern hemispheres. Nature **460**(7254), 491 (2009)

K.M. Laundal, I. Cnossen, S.E. Milan, S. Haaland, J. Coxon, N. Pedatella, M. Förster, J.P. Reistad, North–South asymmetries in Earth's magnetic field. Space Sci. Rev. **206**(1–4), 225–257 (2017)

G. Le, Y. Wang, J. Slavin, R. Strangeway, Space Technology 5 multipoint observations of temporal and spatial variability of field-aligned currents. J. Geophys. Res. Space Phys. **114**(A8), A08206 (2009)

M.R. Lessard, W. Lotko, J. LaBelle, W. Peria, C.W. Carlson, F. Creutzberg, D.D. Wallis, Ground and satellite observations of the evolution of growth phase auroral arcs. J. Geophys. Res. Space Phys. **112**(A9), A09304 (2007). https://doi.org/10.1029/2006JA011794. https://agupubs.onlinelibrary.wiley.com/doi/abs/10.1029/2006JA011794

B. Li, G. Marklund, T. Karlsson, S. Sadeghi, P.-A. Lindqvist, A. Vaivads, A. Fazakerley, Y. Zhang, E. Lucek, T. Sergienko, et al., Inverted-v and low-energy broadband electron acceleration features of multiple auroras within a large-scale surge. J. Geophys. Res. Space Phys. **118**(9), 5543–5552 (2013)

P.-A. Lindqvist, G.T. Marklund, A statistical study of high-altitude electric fields measured on the viking satellite. J. Geophys. Res. Space Phys. **95**(A5), 5867–5876 (1990). https://doi.org/10.1029/JA095iA05p05867

K. Liou, P.T. Newell, C.-I. Meng, M. Brittnacher, G. Parks, Synoptic auroral distribution: a survey using polar ultraviolet imagery. J. Geophys. Res. Space Phys. **102**(A12), 27197–27205 (1997). https://doi.org/10.1029/97JA02638. https://agupubs.onlinelibrary.wiley.com/doi/abs/10.1029/97JA02638

J. Liu, V. Angelopoulos, Z. Yao, X. Chu, X.-Z. Zhou, A. Runov, The current system of dipolarizing flux bundles and their role as wedgelets in the substorm current wedge, in *Electric Currents in Geospace and Beyond*, vol. 235, (Wiley Online Library, New York, 2018a), pp. 323–337

J. Liu, L. Lyons, W. Archer, B. Gallardo-Lacourt, Y. Nishimura, Y. Zou, C. Gabrielse, J. Weygand, Flow shears at the poleward boundary of omega bands observed during conjunctions of swarm and THEMIS ASI. Geophys. Res. Lett. **45**(3), 1218–1227 (2018b). https://doi.org/10.1002/2017GL076485

E. Lund, E. Möbius, R. Ergun, C. Carlson, Mass-dependent effects in ion conic production: the role of parallel electric fields. Geophys. Res. Lett. **26**(24), 3593–3596 (1999)

R. Lundin, D.S. Evans, Boundary layer plasmas as a source for high-latitude, early afternoon, auroral arcs. Planet. Space Sci. **33**(12), 1389–1406 (1985)

R. Lundin, I. Sandahl, Some characteristics of the parallel electric field acceleration of electrons over discrete auroral arcs as observed from two rocket flights, in *European Sounding Rocket, Balloon and Related Research, with Emphasis on Experiments at High Latitudes*, vol. 135 (1978)

K. Lynch, J. Bonnell, C. Carlson, W. Peria, Return current region aurora: $E_{\parallel}$, j_z, particle energization, and broadband ELF wave activity. J. Geophys. Res. Space Phys. **107**(A7), 1115 (2002)

K. Lynch, D. Hampton, M. Zettergren, T. Bekkeng, M. Conde, P. Fernandes, P. Horak, M. Lessard, R. Miceli, R. Michell, et al., Mica sounding rocket observations of conductivity-gradient-generated auroral ionospheric responses: small-scale structure with large-scale drivers. J. Geophys. Res. Space Phys. **120**(11), 9661–9682 (2015)

L. Lyons, D. Evans, R. Lundin, An observed relationship between magnetic field-aligned electric fields and downward electron energy fluxes in the vicinity of auroral forms. J. Geophys. Res. **84**, 457 (1979)

L. Lyons, J. Fennell, A. Vampola, A general association between discrete auroras and ion precipitation from the tail. J. Geophys. Res. Space Phys. **93**(A11), 12932–12940 (1988)

L.R. Lyons, I.O. Voronkov, E.F. Donovan, E. Zesta, Relation of substorm breakup arc to other growth-phase auroral arcs. J. Geophys. Res. Space Phys. **107**(A11), 26–12610 (2002). https://doi.org/10.1029/2002JA009317. https://agupubs.onlinelibrary.wiley.com/doi/abs/10.1029/2002JA009317

R.L. Lysak, Auroral electrodynamics with current and voltage generators. J. Geophys. Res. Space Phys. **90**(A5), 4178–4190 (1985)
R.L. Lysak, Electrodynamic coupling of the magnetosphere and ionosphere. Space Sci. Rev. **52**(1), 33–87 (1990). https://doi.org/10.1007/BF00704239
R.L. Lysak, Propagation of Alfvén waves through the ionosphere: dependence on ionospheric parameters. J. Geophys. Res. **104**, 10017–10030 (1999). https://doi.org/10.1029/1999JA900024
J. Maggs, T. Davis, Measurements of the thicknesses of auroral structures. Planet. Space Sci. **16**(2), 205–209 (1968)
A.J. Mallinckrodt, C.W. Carlson, Relations between transverse electric fields and field-aligned currents. J. Geophys. Res. Space Phys. **83**(A4), 1426–1432 (1978). https://doi.org/10.1029/JA083iA04p01426. https://agupubs.onlinelibrary.wiley.com/doi/abs/10.1029/JA083iA04p01426
Y.P. Maltsev, W.B. Lyatsky, A.M. Lyatskaya, Currents over the auroral arc. Planet. Space Sci. **25**(1), 53–57 (1977). https://doi.org/10.1016/0032-0633(77)90117-9. http://www.sciencedirect.com/science/article/pii/0032063377901179
O. Marghitu, Auroral arc electrodynamics: review and outlook, in *Auroral Phenomenology and Magnetospheric Processes: Earth and Other Planets*, vol. 197 (2012), pp. 143–158
O. Marghitu, B. Klecker, G. Haerendel, J. McFadden, ALADYN: a method to investigate auroral arc electrodynamics from satellite data. J. Geophys. Res. Space Phys. **109**(A11), A11305 (2004)
O. Marghitu, M. Hamrin, B. Klecker, A. Vaivads, J. McFadden, S. Buchert, L.M. Kistler, I. Dandouras, M. André, H. Rème, Experimental investigation of auroral generator regions with conjugate Cluster and FAST data, in *Annales Geophysicae*, vol. 24 (2006), pp. 619–635
O. Marghitu, B. Klecker, J. McFadden, The anisotropy of precipitating auroral electrons: a fast case study. Adv. Space Res. **38**(8), 1694–1701 (2006)
O. Marghitu, T. Karlsson, B. Klecker, G. Haerendel, J. McFadden, Auroral arc and oval electrodynamics in the Harang region. J. Geophys. Res. Space Phys. **114**(A3), A03214 (2009)
O. Marghitu, C. Bunescu, T. Karlsson, B. Klecker, H.C. Stenbaek-Nielsen, On the divergence of the auroral electrojets. J. Geophys. Res. Space Phys. **116**(A1), A00K17 (2011)
G. Marklund, Auroral arc classification scheme based on the observed arc-associated electric field pattern. Planet. Space Sci. **32**(2), 193–211 (1984)
G. Marklund, I. Sandahl, H. Opgenoorth, A study of the dynamics of a discrete auroral arc. Planet. Space Sci. **30**(2), 179–197 (1982). https://doi.org/10.1016/0032-0633(82)90088-5. https://www.sciencedirect.com/science/article/pii/0032063382900885?via%3Dihub
G. Marklund, L. Blomberg, C.-G. Fälthammar, P.-A. Lindqvist, On intense diverging electric fields associated with black aurora. Geophys. Res. Lett. **21**(17), 1859–1862 (1994)
G.T. Marklund, N. Ivchenko, T. Karlsson, A. Fazakerley, M. Dunlop, P.-A. Lindqvist, S. Buchert, C. Owen, M. Taylor, A. Vaivalds, et al., Temporal evolution of the electric field accelerating electrons away from the auroral ionosphere. Nature **414**(6865), 724 (2001)
G.T. Marklund, S. Sadeghi, T. Karlsson, P.-A. Lindqvist, H. Nilsson, C. Forsyth, A. Fazakerley, E.A. Lucek, J. Pickett, Altitude distribution of the auroral acceleration potential determined from cluster satellite data at different heights. Phys. Rev. Lett. **106**(5), 055002 (2011a)
G.T. Marklund, S. Sadeghi, J.A. Cumnock, T. Karlsson, P.-A. Lindqvist, H. Nilsson, A. Masson, A. Fazakerley, E. Lucek, J. Pickett, et al., Evolution in space and time of the quasi-static acceleration potential of inverted-V aurora and its interaction with Alfvénic boundary processes. J. Geophys. Res. Space Phys. **116**(A1), A00K13 (2011b)
I. McCrea, A. Aikio, L. Alfonsi, E. Belova, S. Buchert, M. Clilverd, N. Engler, B. Gustavsson, C. Heinselman, J. Kero, et al., The science case for the EISCAT_3d radar. Prog. Earth Planet. Sci. **2**(1), 21 (2015)
J.P. McFadden, C.W. Carlson, R.E. Ergun, Microstructure of the auroral acceleration region as observed by fast. J. Geophys. Res. Space Phys. **104**(A7), 14453–14480 (1999). https://doi.org/10.1029/1998JA900167. https://agupubs.onlinelibrary.wiley.com/doi/abs/10.1029/1998JA900167
C.E. McIlwain, Direct measurement of particles producing visible auroras. J. Geophys. Res. **65**(9), 2727–2747 (1960)
D. McKay, N. Partamies, J. Vierinen, Pulsating aurora and cosmic noise absorption associated with growth-phase arcs. Ann. Geophys. **36**(1), 59–69 (2018). https://doi.org/10.5194/angeo-36-59-2018. https://www.ann-geophys.net/36/59/2018/
R.L. McPherron, C.T. Russell, M.P. Aubry, Satellite studies of magnetospheric substorms on August 15, 1968: 9. Phenomenological model for substorms. J. Geophys. Res. **78**(16), 3131–3149 (1973)
S. Mende, The THEMIS array of ground-based observatories for the study of auroral substorms. Space Sci. Rev. **141**, 357 (2008). https://doi.org/10.1007/s11214-008-9380-x
S. Mende, R. Eather, Monochromatic all-sky observations and auroral precipitation patterns. J. Geophys. Res. **81**(22), 3771–3780 (1976)

C.-I. Meng, R. Lundin, Auroral morphology of the midday oval. J. Geophys. Res. Space Phys. **91**(A2), 1572–1584 (1986)
D. Miles, I.R. Mann, I. Pakhotin, J.K. Burchill, A.D. Howarth, D.J. Knudsen, R.L. Lysak, D. Wallis, L. Cogger, A. Yau, Alfvénic dynamics and fine structuring of discrete auroral arcs: swarm and e-pop observations. Geophys. Res. Lett. **45**(2), 545–555 (2018)
J. Moen, P. Sandholt, M. Lockwood, A. Egeland, K. Fukui, Multiple, discrete arcs on sunward convecting field lines in the 14-15 MLT region. J. Geophys. Res. Space Phys. **99**(A4), 6113–6123 (1994)
T. Moore, M.-C. Fok, K. Garcia-Sage, The ionospheric outflow feedback loop. J. Atmos. Sol.-Terr. Phys. **115**, 59–66 (2014)
M. Morooka, T. Mukai, Density as a controlling factor for seasonal and altitudinal variations of the auroral particle acceleration region. J. Geophys. Res. Space Phys. **108**(A7), 1306 (2003)
T. Motoba, M. Hirahara, High-resolution auroral acceleration signatures within a highly dynamic onset arc. Geophys. Res. Lett. **43**(5), 1793–1801 (2016). https://doi.org/10.1002/2015GL067580. https://agupubs.onlinelibrary.wiley.com/doi/abs/10.1002/2015GL067580
T. Motoba, S. Ohtani, B.J. Anderson, H. Korth, D. Mitchell, L.J. Lanzerotti, K. Shiokawa, M. Connors, C.A. Kletzing, G.D. Reeves, On the formation and origin of substorm growth phase/onset auroral arcs inferred from conjugate space-ground observations. J. Geophys. Res. Space Phys. **120**(10), 8707–8722 (2015). https://doi.org/10.1002/2015JA021676. https://agupubs.onlinelibrary.wiley.com/doi/abs/10.1002/2015JA021676
F.S. Mozer, A. Hull, Origin and geometry of upward parallel electric fields in the auroral acceleration region. J. Geophys. Res. Space Phys. **106**(A4), 5763–5778 (2001). https://doi.org/10.1029/2000JA900117
F. Mozer, C. Kletzing, Direct observation of large, quasi-static, parallel electric fields in the auroral acceleration region. Geophys. Res. Lett. **25**(10), 1629–1632 (1998)
F.S. Mozer, C.W. Carlson, M. Hudson, R. Torbert, B. Parady, J. Yatteau, M.C. Kelley, Observations of paired electrostatic shocks in the polar magnetosphere. Phys. Rev. Lett. **38**(6), 292 (1977)
F.S. Mozer, C. Cattell, M. Hudson, R. Lysak, M. Temerin, R. Torbert, Satellite measurements and theories of low altitude auroral particle acceleration. Space Sci. Rev. **27**(2), 155–213 (1980)
H. Nevanlinna, T.I. Pulkkinen, Auroral observations in Finland: results from all-sky cameras, 1973–1997. J. Geophys. Res. Space Phys. **106**(A5), 8109–8118 (2001). https://doi.org/10.1029/1999JA000362. https://agupubs.onlinelibrary.wiley.com/doi/abs/10.1029/1999JA000362
P.T. Newell, Y.I. Feldstein, Y.I. Galperin, C.-I. Meng, Morphology of nightside precipitation. J. Geophys. Res. Space Phys. **101**(A5), 10737–10748 (1996)
P.T. Newell, K.M. Lyons, C.-I. Meng, A large survey of electron acceleration events. J. Geophys. Res. Space Phys. **101**(A2), 2599–2614 (1996a). https://doi.org/10.1029/95JA03147. https://agupubs.onlinelibrary.wiley.com/doi/abs/10.1029/95JA03147
P.T. Newell, C.-I. Meng, K.M. Lyons, Suppression of discrete aurorae by sunlight. Nature **381**(6585), 766–767 (1996b). https://doi.org/10.1038/381766a0. http://www.nature.com/articles/381766a0
P.T. Newell, R.A. Greenwald, J.M. Ruohoniemi, The role of the ionosphere in aurora and space weather. Rev. Geophys. **39**(2), 137–149 (2001)
P.T. Newell, T. Sotirelis, S. Wing, Diffuse, monoenergetic, and broadband aurora: the global precipitation budget. J. Geophys. Res. Space Phys. **114**(A9) A09207, (2009). https://doi.org/10.1029/2009JA014326. http://doi.wiley.com/10.1029/2009JA014326
P.T. Newell, T. Sotirelis, S. Wing, Seasonal variations in diffuse, monoenergetic, and broadband aurora. J. Geophys. Res. Space Phys. **115**(A3), A03216 (2010). https://doi.org/10.1029/2009JA014805. https://agupubs.onlinelibrary.wiley.com/doi/abs/10.1029/2009JA014805
M.J. Nicolls, S.L. Vadas, J.W. Meriwether, M.G. Conde, D. Hampton, The phases and amplitudes of gravity waves propagating and dissipating in the thermosphere: application to measurements over Alaska. J. Geophys. Res. Space Phys. **117**(A5), A03216 (2012). https://doi.org/10.1029/2012JA017542. https://agupubs.onlinelibrary.wiley.com/doi/abs/10.1029/2012JA017542
H. Nilsson, A. Kozlovsky, T. Sergienko, A. Kotikov, Radar observations in the vicinity of pre-noon auroral arcs. Ann. Geophys. **23**(5), 1785–1796 (2005). https://doi.org/10.5194/angeo-23-1785-2005. http://www.ann-geophys.net/23/1785/2005/
Y. Nishimura, L.R. Lyons, V. Angelopoulos, T. Kikuchi, S. Zou, S.B. Mende, Relations between multiple auroral streamers, pre-onset thin arc formation, and substorm auroral onset. J. Geophys. Res. Space Phys. **116**(A9), A09214 (2011). https://doi.org/10.1029/2011JA016768. https://agupubs.onlinelibrary.wiley.com/doi/abs/10.1029/2011JA016768
Y. Nishimura, L.R. Lyons, T. Kikuchi, V. Angelopoulos, E.F. Donovan, S.B. Mende, H. Lühr, Relation of substorm pre-onset arc to large-scale field-aligned current distribution. Geophys. Res. Lett. **39**(22), L22101 (2012). https://doi.org/10.1029/2012GL053761. https://agupubs.onlinelibrary.wiley.com/doi/abs/10.1029/2012GL053761

Y. Nishimura, L.R. Lyons, M.J. Nicolls, D.L. Hampton, R.G. Michell, M. Samara, W.A. Bristow, E.F. Donovan, E. Spanswick, V. Angelopoulos, S.B. Mende, Coordinated ionospheric observations indicating coupling between preonset flow bursts and waves that lead to substorm onset. J. Geophys. Res. Space Phys. **119**(5), 3333–3344 (2014). https://doi.org/10.1002/2014JA019773. https://agupubs.onlinelibrary.wiley.com/doi/abs/10.1002/2014JA019773

Y. Obuchi, T. Sakanoi, K. Asamura, A. Yamazaki, Y. Kasaba, M. Hirahara, Y. Ebihara, S. Okano, Fine-scale dynamics of black auroras obtained from simultaneous imaging and particle observations with the reimei satellite. J. Geophys. Res. Space Phys. **116**(A1), A00K07 (2011)

N. Østgaard, N. Tsyganenko, S. Mende, H. Frey, T. Immel, M. Fillingim, L. Frank, J. Sigwarth, Observations and model predictions of substorm auroral asymmetries in the conjugate hemispheres. Geophys. Res. Lett. **32**(5) (2005). https://doi.org/10.1029/2004GL022166

N. Østgaard, J.P. Reistad, P. Tenfjord, K.M. Laundal, K. Snekvik, S. Milan, S. Haaland, Mechanisms that produce auroral asymmetries in conjugate hemispheres, in *Auroral Dynamics and Space Weather*, vol. 215 (2015), p. 133

N. Partamies, P. Janhunen, K. Kauristie, S. Mäkinen, T. Sergienko, Testing an inversion method for estimating electron energy fluxes from all-sky camera images. Ann. Geophys. **22**, 1961–1971 (2004). https://doi.org/10.5194/angeo-22-1961-2004

N. Partamies, E. Donovan, D. Knudsen, Statistical study of inverted-V structures in FAST data. Ann. Geophys. **26**, 1439–1449 (2008). www.ann-geophys.net/26/1439/2008/

N. Partamies, M. Syrjäsuo, E. Donovan, M. Connors, D. Charrois, D. Knudsen, Z. Kryzanowsky, Observations of the auroral width spectrum at kilometre-scale size. Ann. Geophys. **28**, 711–718 (2010). www.ann-geophys.net/28/711/2010/

N. Partamies, D. Whiter, M. Syrjäsuo, K. Kauristie, Solar cycle and diurnal dependence of auroral structures. J. Geophys. Res. Space Phys. **119**(10), 8448–8461 (2014). https://doi.org/10.1002/2013JA019631. https://agupubs.onlinelibrary.wiley.com/doi/abs/10.1002/2013JA019631

N. Partamies, L. Juusola, D. Whiter, K. Kauristie, Substorm evolution of auroral structures. J. Geophys. Res. Space Phys. **120**(7), 5958–5972 (2015). https://doi.org/10.1002/2015JA021217. https://agupubs.onlinelibrary.wiley.com/doi/abs/10.1002/2015JA021217

G. Paschmann, S. Haaland, R. Treumann, *Auroral Plasma Physics* (2003)

L. Peticolas, T. Hallinan, H. Stenbaek-Nielsen, J. Bonnell, C. Carlson, A study of black aurora from aircraft-based optical observations and plasma measurements on fast. J. Geophys. Res. Space Phys. **107**(A8), 1217 (2002)

T.I. Pulkkinen, E.I. Tanskanen, A. Viljanen, N. Partamies, K. Kauristie, Auroral electrojets during deep solar minimum at the end of solar cycle 23. J. Geophys. Res. Space Phys. **116**(A4), A04207 (2011). https://doi.org/10.1029/2010JA016098. https://agupubs.onlinelibrary.wiley.com/doi/abs/10.1029/2010JA016098

Q. Qiu, H.-G. Yang, Q.-M. Lu, Q.-H. Zhang, D.-S. Han, Z.-J. Hu, Widths of dayside auroral arcs observed at the Chinese yellow river station. J. Atmos. Sol.-Terr. Phys. **102**, 222–227 (2013). https://doi.org/10.1016/j.jastp.2013.06.002. http://www.sciencedirect.com/science/article/pii/S1364682613001752

Q. Qiu, H.-G. Yang, Q.-M. Lu, Z.-J. Hu, D.-S. Han, Q. Wang, Orientation variation of dayside auroral arc alignments obtained from all-sky observation at yellow river station, svalbard. J. Atmos. Sol.-Terr. Phys. **142**, 20–24 (2016). https://doi.org/10.1016/j.jastp.2016.02.019. http://www.sciencedirect.com/science/article/pii/S1364682616300505

A.J. Ridley, Y. Deng, G. Tóth, The global ionosphere-thermosphere model. J. Atmos. Sol.-Terr. Phys. **68**(8), 839–864 (2006). https://doi.org/10.1016/j.jastp.2006.01.008. http://www.sciencedirect.com/science/article/pii/S1364682606000071

R. Robinson, R. Vondrak, K. Miller, T. Dabbs, D. Hardy, On calculating ionospheric conductances from the flux and energy of precipitating electrons. J. Geophys. Res. Space Phys. **92**(A3), 2565–2569 (1987)

G. Rostoker, R. Boström, A mechanism for driving the Gross Birkeland current configuration in the auroral oval. J. Geophys. Res. **81**(1), 235–244 (1976)

S. Sadeghi, M. Emami, Large-scale altitude distribution profile of auroral parallel electric potentials: a statistical analysis of cluster data. Adv. Space Res. **64**(2), 378–384 (2019)

S. Sadeghi, G.T. Marklund, T. Karlsson, P.-A. Lindqvist, H. Nilsson, O. Marghitu, A. Fazakerley, E.A. Lucek, Spatiotemporal features of the auroral acceleration region as observed by cluster. J. Geophys. Res. Space Phys. **116**(A1) (2011). https://doi.org/10.1029/2011JA016505

V.V. Safargaleev, A.E. Kozlovsky, S.V. Osipenko, V.R. Tagirov, Azimuthal expansion of high-latitude auroral arcs. Ann. Geophys. **21**(8), 1793–1805 (2003). https://doi.org/10.5194/angeo-21-1793-2003. https://www.ann-geophys.net/21/1793/2003/

T. Sakanoi, Y. Obuchi, Y. Ebihara, Y. Miyoshi, K. Asamura, A. Yamazaki, Y. Kasaba, M. Hirahara, T. Nishiyama, S. Okano, *Fine-Scale Characteristics of Black Aurora and Its Generation Process*. Geophysical Monograph Series, vol. 197 (Am. Geophys. Union, Washington, 2012)

P.E. Sandholt, H.C. Carlson, A. Egeland, *Dayside and Polar Cap Aurora*, vol. 270 (Springer, Berlin, 2006)

L. Sangalli, B. Gustavsson, N. Partamies, K. Kauristie, Estimating the peak auroral emission altitude from all-sky images. Opt. Pura Apl. **44**, 593–598 (2011)

T.E. Sarris, E. R. Talaat, M. Palmroth, I. Dandouras, E. Armandillo, G. Kervalishvili, S. Buchert, D. Malaspina, A. Jaynes, N. Paschalidis, J. Sample, J. Halekas, S. Tourgaidis, V. Lappas, M. Clilverd, Q. Wu, I. Sandberg, A. Aikio, P. Pirnaris, Daedalus: a low-flying spacecraft for the exploration of the lower thermosphere—Ionosphere. Geoscientific Instrumentation, Methods and Data Systems Discussions, 1–59 (2019). https://doi.org/10.5194/gi-2019-3

N. Sato, T. Nagaoka, K. Hashimoto, T. Saemundsson, Conjugacy of isolated auroral arcs and nonconjugate auroral breakups. J. Geophys. Res. Space Phys. **103**(A6), 11641–11652 (1998)

N. Sato, A. Kadokura, T. Motoba, K. Hosokawa, G. Björnsson, T. Saemundsson, Interhemispheric symmetries and asymmetries of aurora from ground-based conjugate observations, in *Auroral Dynamics and Space Weather*, vol. 215 (2015), p. 145

J. Semeter, T. Butler, M. Zettergren, C. Heinselman, M. Nicolls, Composite imaging of auroral forms and convective flows during a substorm cycle. J. Geophys. Res. Space Phys. **115**(A8) (2010). https://doi.org/10.1029/2009JA014931

V. Sergeev, Y. Nishimura, M. Kubyshkina, V. Angelopoulos, R. Nakamura, H. Singer, Magnetospheric location of the equatorward prebreakup arc. J. Geophys. Res. Space Phys. **117**(A1), A01212 (2012). https://doi.org/10.1029/2011JA017154. https://agupubs.onlinelibrary.wiley.com/doi/abs/10.1029/2011JA017154

J. Sesiano, P. Cloutier, Measurements of field-aligned currents in a multiple auroral arc system. J. Geophys. Res. **81**(1), 116–122 (1976)

Y. Shen, D.J. Knudsen, J.K. Burchill, A.D. Howarth, A.W. Yau, D.M. Miles, H.G. James, G.W. Perry, L. Cogger, Low-altitude ion heating, downflowing ions, and BBELF waves in the return current region. J. Geophys. Res. Space Phys. **123**(4), 3087–3110 (2018). https://doi.org/10.1002/2017JA024955

K. Shiokawa, K. Yago, K. Yumoto, D.G. Baishev, S.I. Solovyev, F.J. Rich, S.B. Mende, Ground and satellite observations of substorm onset arcs. J. Geophys. Res. Space Phys. **110**(A12), A12225 (2005). https://doi.org/10.1029/2005JA011281. https://agupubs.onlinelibrary.wiley.com/doi/abs/10.1029/2005JA011281

C. Simon Wedlund, H. Lamy, B. Gustavsson, T. Sergienko, U. Brändström, Estimating energy spectra of electron precipitation above auroral arcs from ground-based observations with radar and optics. J. Geophys. Res. Space Phys. **118**(6), 3672–3691 (2013). https://doi.org/10.1002/jgra.50347. https://agupubs.onlinelibrary.wiley.com/doi/abs/10.1002/jgra.50347

K. Stasiewicz, T. Potemra, Multiscale current structures observed by Freja. J. Geophys. Res. Space Phys. **103**(A3), 4315–4325 (1998). https://doi.org/10.1029/97JA02396. http://doi.wiley.com/10.1029/97JA02396

H.C. Stenbaek-Nielsen, T.J. Hallinan, D.L. Osborne, J. Kimball, C. Chaston, J. McFadden, G. Delory, M. Temerin, C.W. Carlson, Aircraft observations conjugate to fast: auroral are thicknesses. Geophys. Res. Lett. **25**(12), 2073–2076 (1998). https://doi.org/10.1029/98GL01058. https://agupubs.onlinelibrary.wiley.com/doi/abs/10.1029/98GL01058

R. Strangeway, R. Ergun, Y.-J. Su, C. Carlson, R. Elphic, Factors controlling ionospheric outflows as observed at intermediate altitudes. J. Geophys. Res. Space Phys. **110**(A3), A03221 (2005)

A.V. Streltsov, Effects of ionospheric heating on feedback-unstable electromagnetic waves. J. Geophys. Res. Space Phys. **113**(A9) A09211, (2008). https://doi.org/10.1029/2008JA013199. http://doi.wiley.com/10.1029/2008JA013199

M. Sugiura, A fundamental magnetosphere-ionosphere coupling mode involving field-aligned currents as deduced from DE-2 observations. Geophys. Res. Lett. **11**(9), 877–880 (1984)

D.W. Swift, D.J. Gorney, Production of very energetic electrons in discrete aurora. J. Geophys. Res. **94**(A3), 2696 (1989). https://doi.org/10.1029/JA094iA03p02696. http://doi.wiley.com/10.1029/JA094iA03p02696

M.T. Syrjäsuo, E.F. Donovan, Diurnal auroral occurrence statistics obtained via machine vision. Ann. Geophys. **22**(4), 1103–1113 (2004). https://doi.org/10.5194/angeo-22-1103-2004. https://www.ann-geophys.net/22/1103/2004/

J.R. Thieman, R.A. Hoffman, Determination of inverted-v stability from dynamics explorer satellite data. J. Geophys. Res. Space Phys. **90**(A4), 3511–3516 (1985)

T. Trondsen, L. Cogger, High-resolution television observations of black aurora. J. Geophys. Res. Space Phys. **102**(A1), 363–378 (1997)

H. Vanhamäki, O. Amm, Analysis of ionospheric electrodynamic parameters on mesoscales-a review of selected techniques using data from ground-based observation networks and satellites, in *Annales Geophysicae*, vol. 29 (2011), p. 467. Copernicus GmbH

J. Vogt, Alfvén wave coupling in the auroral current circuit. Surv. Geophys. **23**(4), 335–377 (2002)

R. Vondrak, S. Harris, S. Mende, Ground-based observations of subauroral energetic-electron arcs. Geophys. Res. Lett. **10**(7), 557–560 (1983)

J. Vogt, G. Haerendel, K. Glassmeier, A model for the reflection of Alfvén waves at the source region of the Birkeland current system: the tau generator. J. Geophys. Res. Space Phys. **104**(A1), 269–278 (1999a)

J. Vogt, H. Frey, G. Haerendel, H. Höfner, J. Semeter, Shear velocity profiles associated with auroral curls. J. Geophys. Res. Space Phys. **104**(A8), 17277–17288 (1999b)

J.A. Wanliss, J.C. Samson, E. Friedrich, On the use of photometer data to map dynamics of the magnetotail current sheet during substorm growth phase. J. Geophys. Res. Space Phys. **105**(A12), 27673–27684 (2000). https://doi.org/10.1029/2000JA000178. https://agupubs.onlinelibrary.wiley.com/doi/abs/10.1029/2000JA000178

D.R. Weimer, D.A. Gurnett, Large-amplitude auroral electric fields measured with DE 1. J. Geophys. Res. Space Phys. **98**(A8), 13557–13564 (1993). https://doi.org/10.1029/93JA00793

D.R. Weimer, C. Goertz, D. Gurnett, N. Maynard, J. Burch, Auroral zone electric fields from DE 1 and 2 at magnetic conjunctions. J. Geophys. Res. Space Phys. **90**(A8), 7479–7494 (1985)

D.K. Whiter, B.S. Lanchester, T. Sakanoi, K. Asamura, Estimating high-energy electron fluxes by intercalibrating reimei optical and particle measurements using an ionospheric model. J. Atmos. Sol.-Terr. Phys. **89**, 8–17 (2012). https://doi.org/10.1016/j.jastp.2012.06.014. http://www.sciencedirect.com/science/article/pii/S136468261200168X

A.N. Wright, C.J. Owen, C.C. Chaston, M.W. Dunlop, Downward current electron beam observed by cluster and fast. J. Geophys. Res. Space Phys. **113**(A6), A06202 (2008)

J. Wu, D. Knudsen, D. Gillies, E. Donovan, J. Burchill, Swarm observation of field-aligned currents associated with multiple auroral arc systems. J. Geophys. Res. Space Phys. **122**(10), 10145–10156 (2017)

J. Wygant, A. Keiling, C. Cattell, l.M. Johnson, R. Lysak, M. Temerin, F. Mozer, C. Kletzing, J. Scudder, W. Peterson, et al., Polar spacecraft based comparisons of intense electric fields and poynting flux near and within the plasma sheet-tail lobe boundary to uvi images: an energy source for the aurora. J. Geophys. Res. Space Phys. **105**(A8), 18675–18692 (2000)

K. Yago, K. Shiokawa, K. Hayashi, K. Yumoto, Auroral particles associated with a substorm brightening arc. Geophys. Res. Lett. **32**(6), L06104 (2005). https://doi.org/10.1029/2004GL021894. https://agupubs.onlinelibrary.wiley.com/doi/abs/10.1029/2004GL021894

A. Yoshikawa, Excitation of a Hall-current generator by field-aligned current closure, via an ionospheric, divergent Hall-current, during the transient phase of magnetosphere–ionosphere coupling. J. Geophys. Res. Space Phys. **107**(A12), 1445 (2002a). https://doi.org/10.1029/2001JA009170

A. Yoshikawa, How does the ionospheric rotational Hall current absorb the increasing energy from the field-aligned current system? Geophys. Res. Lett. **29**(7), 37 (2002b)

A. Yoshikawa, R. Fujii, Earth's ionosphere: theory and phenomenology of Cowling channels, in *Electric Currents in Geospace and Beyond*, vol. 235 (Wiley Online Library, New York, 2018), pp. 427–443

A. Yoshikawa, O. Amm, H. Vanhamäki, R. Fujii, Illustration of Cowling channel coupling to the shear Alfven wave. J. Geophys. Res. Space Phys. **118**(10), 6405–6415 (2013)

A. Yoshikawa, O. Amm, H. Vanhamäki, A. Nakamizo, R. Fujii, Theory of Cowling channel formation by reflection of shear Alfven waves from the auroral ionosphere. J. Geophys. Res. Space Phys. **118**(10), 6416–6425 (2013)

M. Zettergren, J. Semeter, Ionospheric plasma transport and loss in auroral downward current regions. J. Geophys. Res. Space Phys. **117**(A6) A06306, (2012). https://doi.org/10.1029/2012JA017637. http://doi.wiley.com/10.1029/2012JA017637

M. Zettergren, J. Semeter, Ionospheric plasma transport and loss in auroral downward current regions. J. Geophys. Res. Space Phys. **117**(A16), 6306 (2012). https://doi.org/10.1029/2012JA017637

M. Zettergren, J. Semeter, Ionospheric plasma transport and loss in auroral downward current regions. J. Geophys. Res. Space Phys. **117**(A6), A06306 (2012)

M.D. Zettergren, J.B. Snively, Ionospheric response to infrasonic-acoustic waves generated by natural hazard events. J. Geophys. Res. Space Phys. **120**(9), 8002–8024 (2015). https://doi.org/10.1002/2015JA021116. https://agupubs.onlinelibrary.wiley.com/doi/abs/10.1002/2015JA021116

M.D. Zettergren, J.B. Snively, Latitude and longitude dependence of ionospheric tec and magnetic perturbations from infrasonic-acoustic waves generated by strong seismic events. Geophys. Res. Lett. **46**(3), 1132–1140 (2019). https://doi.org/10.1029/2018GL081569. https://agupubs.onlinelibrary.wiley.com/doi/abs/10.1029/2018GL081569

M. Zettergren, K. Lynch, D. Hampton, M. Nicolls, B. Wright, M. Conde, J. Moen, M. Lessard, R. Miceli, S. Powell, Auroral ionospheric f region density cavity formation and evolution: MICA campaign results. J. Geophys. Res. Space Phys. **119**(4), 3162–3178 (2014)

M.D. Zettergren, J.L. Semeter, H. Dahlgren, Dynamics of density cavities generated by frictional heating: formation, distortion, and instability. Geophys. Res. Lett. **42**(23), 10120–10125 (2015). https://doi.org/10.1002/2015GL066806. https://agupubs.onlinelibrary.wiley.com/doi/abs/10.1002/2015GL066806

L. Zheng, S. Fu, Q. Zong, G. Parks, C. Wang, X. Chen, Solar cycle dependence of the seasonal variation of auroral hemispheric power. Chin. Sci. Bull. **58**(4), 525–530 (2013). https://doi.org/10.1007/s11434-012-5378-6

S. Zou, L.R. Lyons, M.J. Nicolls, C.J. Heinselman, S.B. Mende, Nightside ionospheric electrodynamics associated with substorms: PFISR and THEMIS ASI observations. J. Geophys. Res. Space Phys. **114**(A12), A12301 (2009a). https://doi.org/10.1029/2009JA014259. https://agupubs.onlinelibrary.wiley.com/doi/abs/10.1029/2009JA014259

S. Zou, L. Lyons, C.-P. Wang, A. Boudouridis, J. Ruohoniemi, P. Anderson, P. Dyson, J. Devlin, On the coupling between the Harang reversal evolution and substorm dynamics: a synthesis of SuperDARN, DMSP, and IMAGE observations. J. Geophys. Res. Space Phys. **114**(A1), A01205 (2009b)

S. Zou, L.R. Lyons, Y. Nishimura, *Mutual Evolution of Aurora and Ionospheric Electrodynamic Features Near the Harang Reversal During Substorms*. Geophysical Monograph Series, vol. 197 (Am. Geophys. Union, Washington, 2012). https://doi.org/10.1029/2011GM001163

Y. Zou, Y. Nishimura, L. Lyons, M. Conde, R. Varney, V. Angelopoulos, S. Mende, Mesoscale *F* region neutral winds associated with quasi-steady and transient nightside auroral forms. J. Geophys. Res. Space Phys. **123**(9), 7968–7984 (2018). https://doi.org/10.1029/2018JA025457. http://doi.wiley.com/10.1029/2018JA025457